Title page **June 26, 2019**

Motor cortex can directly drive the globus pallidal neurons in a projection neuron type dependent manner in rat

Fuyuki Karube[1]*, Susumu Takahashi[1,2], Kenta Kobayashi[3], and Fumino Fujiyama[1]*

[1] Laboratory of Neural Circuitry, Graduate School of Brain Science, Doshisha University
Kyotanabe 610-0394, Japan

[2] Laboratory of Cognitive and Behavioral Neuroscience, Graduate School of Brain Science, Doshisha University
Kyotanabe 610-0394, Japan (Current address)

[3] Section of Viral Vector Development, National Institute for Physiological Sciences
Okazaki 444-8585, Japan

***Correspondence to:** Associate Prof. Fuyuki Karube and Prof. Fumino Fujiyama
Laboratory of Neural Circuitry
Graduate School of Brain Science, Doshisha University
Kyotanabe 610-0394, JAPAN

Tel: 81-774-65-7381 (Japan)

Fax: 81-774-73-1931

E-mail: fkarube@mail.doshisha.ac.jp

ffujiyam@mail.doshisha.ac.jp

Author contributions

FK designed and performed all experiments and analyzed the data. KK prepared the viral vectors. FK, ST, and FF contributed reagents, experimental devices, and tools. FK, ST, and FF wrote the manuscript.

Declarations of interest

The authors declare no competing financial interests.

Short title: A cell type-dependent cortico-pallidal pathway

Key words: cerebral cortex, globus pallidus, striatum, subthalamic nucleus, projection

Number of tables: 1

Number of figures: 10 figures and 4 figure-figure supplements.

Number of supplementary materials: 2 supplementary tables and 2 supplementary figures.

Acknowledgement: The authors thank Dr. Yasuharu Hirai for discussion and comments. We also thank Dr. Yoon-Mi Oh for technical assistance.

Grant information: This study was funded by Grants-in-Aid from The Ministry of Education, Culture, Sports, Science, and Technology (MEXT) and Japan Society for the Promotion of Science (JSPS) for Scientific Research (26350983 and 16H01622 to FK; 16H06543, 16H02840 to ST; 25282247 and 15K12770 to FF) and for Scientific Researches on Innovative Areas “Adaptive Circuit Shift” (26112001 to FF).

52 **Abbreviations:**

53 A/P, anterior/posterior coordinate; ACSF, artificial cerebrospinal fluid; AP5,
54 5-aminophosphonovaleric acid; BDA, biotinylated dextran amine; CB, calbindin; CC, cingulate
55 cortex; ChR2, channel rhodopsin 2; CMAc, caudal cingulate motor area; CMAr, rostral cingulate
56 motor area; CNQX, 6-cyano-7-nitroquinoxaline-2,3-dione; CTB, cholera toxin subunit B; D/V,
57 dorsal/ventral coordinate; DAB, 3,3′ -diaminobenzidine; EP, entopeduncular nucleus; EPSC,
58 excitatory postsynaptic current; fAHP, fast afterhyperpolarization; FoxP2, forkhead box protein 2;
59 GABA, gamma aminobutyric acid; GP, globus pallidus external segment in rodents; GP_{Bi},
60 bi-directionally projecting GP neurons; GP_{CPu}, GP neurons projecting to the striatum; GP_{STN}, GP
61 neurons projecting to the STN; ic, internal capsule; LED, light-emitting diode; Lhx6, LIM homeobox
62 6; LO, lateral orbitofrontal area; M/L, mediolateral coordinate; MOR, mu-opioid receptor; MSN,
63 medium spiny neuron; N.A., numerical aperture; oEPSC, optically evoked EPSC; OFC, orbitofrontal
64 cortex; PB, phosphate buffer; PHA-L, Phaseolus vulgaris leucoagglutinin; PT, pyramidal tract; PV,
65 parvalbumin; ROI, region of interest; RT, room temperature; sAHP, slow afterhyperpolarization;
66 SMA, supplementary motor area; SN, substantia nigra; SNc, substantia nigra pars compacta; SNr,
67 substantia nigra pars reticulata; STN, subthalamic nucleus; TBS, Tris buffered saline; TTX,
68 tetrodotoxin.
69

Abstract

The basal ganglia (BG) are critical for the control of motor behaviors and for reinforcement learning. Here, we demonstrate in rats that primary and secondary motor areas (M1 and M2) make functional synaptic connections in the globus pallidus (GP), not usually thought of as an input site of the BG using optogenetics and morphological analysis. The cortical excitation in the GP was as strong as that in the STN. GP neurons projecting to the striatum were preferentially innervated by the motor cortex. Morphological observation revealed that the density of axonal boutons from motor cortices in the GP was approximately 30% of that in the striatum, but was comparable to that in the STN. M1 and M2 projected differentially to the BG in terms of topography and substructures. These results suggest that cortico-pallidal innervation is an additional excitatory input to the BG, and can affects behaviors via the cortex-basal ganglia-thalamus loop.

Introduction

Parallel loops of neural connections among the cerebral cortex, basal ganglia, and thalamus contribute to multiple aspects of behavior (Alexander, DeLong, & Strick, 1986; Nambu, 2008; Wei & Wang, 2016). The functions mediated by these loops depend on relevant cortical areas and brain regions receiving outputs of the basal ganglia (Hikosaka, 2007; Middleton & Strick, 2000). The loop containing the motor cortex is crucial for appropriate motor control, action selection, and movement-related learning. Dysfunction of the motor loop involves movement disorders such as

89 Parkinsonian disease (Albin, Young, & Penney, 1989; DeLong, 1990; Middleton & Strick, 2002;
90 Nambu, 2008; Nambu et al., 2000; Parent & Hazrati, 1995a; Redgrave et al., 2010; Wichmann &
91 DeLong, 1996). Cortical projections drive three pathways in the basal ganglia: the direct, the indirect,
92 and the hyperdirect pathways (Bolam, Hanley, Booth, & Bevan, 2000; Y. Smith, Bevan, Shink, &
93 Bolam, 1998). The direct and indirect pathways are mediated by two distinct types of striatal
94 medium spiny neurons (MSNs), termed the direct- and indirect-pathway MSNs (dMSNs and iMSNs).
95 dMSNs project to the output nuclei of the basal ganglia, namely the substantia nigra (SN) pars
96 reticulata (SNr), and the globus pallidus internal segment, the latter termed the entopeduncular
97 nucleus (EP) in rodents. The iMSNs project to the globus pallidus external segment (GP in rodents),
98 which interconnects with the subthalamic nucleus (STN). In turn, both STN and GP also innervate
99 the output nuclei. The hyperdirect pathway involves direct cortical projections to the STN (Nambu,
100 Tokuno, & Takada, 2002), which provides the fastest information flow among the three pathways
101 (Nambu et al., 2000). The behavioral functions of these pathways are gradually being elucidated,
102 although recent findings propose refinement and reappraisal of the classical views of the functional
103 roles of distinct MSNs (Calabresi, Picconi, Tozzi, Ghiglieri, & Di Filippo, 2014; Cui et al., 2013;
104 Isomura et al., 2013; Vicente, Galvao-Ferreira, Tecuapetla, & Costa, 2016). According to the
105 traditional model, the direct pathway promotes the execution of desired actions, whereas the indirect
106 pathway prevents the execution of competing actions (Friend & Kravitz, 2014; Nambu, 2007;
107 Vicente et al., 2016), and the hyperdirect pathway emergently cancels or switches imminent

movements (Frank, Samanta, Moustafa, & Sherman, 2007; Isoda & Hikosaka, 2008; Nambu et al., 2002; Schmidt, Leventhal, Mallet, Chen, & Berke, 2013). In this regard, basal ganglia activity and function are likely modulated by the cerebral cortex.

The rodent motor cortical area is composed of primary and secondary motor cortices, M1 and M2, respectively. The rodent M1 codes and conducts movement signals (Barth, Jones, & Schallert, 1990; Brown & Teskey, 2014) via direct projections to the brainstem and spinal cord, analogously to the primate M1. It has been debated whether the rodent M2, which has various other names such as the medial agranular cortex and the medial precentral cortex (Ebbesen et al., 2018; Svoboda & Li, 2018), is a functional counterpart of the primate premotor and/or supplementary motor areas (Barthas & Kwan, 2017; Svoboda & Li, 2018). Recent studies have revealed the functional role and significance of the rodent M2 (Guo et al., 2014; Hira et al., 2014; Hira et al., 2013; Li, Chen, Guo, Gerfen, & Svoboda, 2015; Manita et al., 2015; D. Miyamoto et al., 2016; Murakami, Shteingart, Loewenstein, & Mainen, 2017; Murakami, Vicente, Costa, & Mainen, 2014; Saiki et al., 2014; Soma et al., 2017; Sul, Jo, Lee, & Jung, 2011). The M2 integrates motor signals and multimodal sensory/internal state information [for review see Barthas and Kwan (2017)]. The M2 is also involved in the preparatory and movement phases of behavior (Guo et al., 2014; Heindorf, Arber, & Keller, 2018; Li et al., 2015; Murakami et al., 2017; Murakami et al., 2014), and learning of motor tasks (Cao et al., 2015; Kawai et al., 2015). Other frontal cortical areas are also related to motor behaviors, such as the orbitofrontal cortex and the cingulate motor area (Bissonette, Powell, &

Roesch, 2013; Friedman et al., 2015; Nakayama, Yokoyama, & Hoshi, 2015; Passingham & Wise, 2012; Paus, 2001; Schoenbaum, Roesch, Stalnaker, & Takahashi, 2009; Sul, Kim, Huh, Lee, & Jung, 2010). The neural circuitry underlying these functional roles and its effects on the basal ganglia and other subcortical regions are not fully known.

Neuron-type diversity is an important factor to understand the neural circuitry. It has been established that distinct neural types other than striatal dMSNs and iMSNs are present in the GP (Abdi et al., 2015; Abrahao & Lovinger, 2018; Cooper & Stanford, 2000; Dodson et al., 2015; Gittis et al., 2014; Hegeman, Hong, Hernandez, & Chan, 2016; Hernandez et al., 2015; H. Kita, 2007; Mallet et al., 2012; Mastro, Bouchard, Holt, & Gittis, 2014), EP (Y. Miyamoto & Fukuda, 2015; Wallace et al., 2017), STN (Baufreton et al., 2003; Xiao et al., 2015), and SN (Kim, Ghazizadeh, & Hikosaka, 2014; Lerner et al., 2015; Matsumoto & Hikosaka, 2009; Menegas et al., 2015). These neuronal populations differ in molecular profile, projection targets, and synaptic inputs. In addition, each nucleus of the basal ganglia contains functional/morphological subdomains (Crittenden & Graybiel, 2011; Fujiyama, Takahashi, & Karube, 2015; Hontanilla, Parent, de las Heras, & Gimenez-Amaya, 1998; H. Kita & Kita, 2001; Parent, Fortin, Cote, & Cicchetti, 1996) correlated with the distribution of glutamatergic innervation (Crittenden & Graybiel, 2011; Eblen & Graybiel, 1995; Fujiyama, Unzai, Nakamura, Nomura, & Kaneko, 2006; Kincaid & Wilson, 1996; J. B. Smith et al., 2016). Even if innervated by the same set of cortical inputs, each cell type can behave differently, recruit distinct neural circuitry, and lead to various behavioral outputs. Therefore, any

account of the functionality of cortical projections to the basal ganglia must consider cell type and subregion.

Cortico-basal ganglia projections are topographically and somatotopically organized (Crittenden & Graybiel, 2011; Gabbott, Warner, Jays, Salway, & Busby, 2005; Nambu, 2011; Shipp, 2016; Voorn, Vanderschuren, Groenewegen, Robbins, & Pennartz, 2004). In the rodent, frontal cortical areas project to the dorsal striatum (Barth et al., 1990; Ebrahimi, Pochet, & Roger, 1992; Reep & Corwin, 1999; Reep et al., 2008; Rouiller, Moret, & Liang, 1993). Recently, topographical maps of cortico-striatal projections have been described in detail (Hintiryan et al., 2016; Hunnicutt et al., 2016; Mailly, Aliane, Groenewegen, Haber, & Deniau, 2013). Cortical projections to the striatum are dependent on the neuron type of origin (Hooks et al., 2018) and individual cortical neurons generally project to multiple sites (T. Kita & Kita, 2012; Shepherd, 2013; Shibata, Tanaka, Hioki, & Furuta, 2018; but see alsoY. Smith, Wichmann, & DeLong, 2014). Thus, basal ganglia nuclei innervated by the same or different cortical areas can be affected simultaneously, in turn, their activities are modulated via the intra-basal ganglia circuitry (Bogacz, Martin Moraud, Abdi, Magill, & Baufreton, 2016; Wei & Wang, 2016). The aim of the present study was to investigate cortical projections to multiple nuclei in the basal ganglia from two motor areas, M1 and M2, in a subregion- and cell type-specific manner. Using a combination of neural tracing with immunofluorescence, we demonstrate that M1 and M2 project to different subregions of each basal ganglia nucleus, and that in the GP, cortical axon collaterals and boutons have topographic distributions that depend on the

cortical area of origin (Naito & Kita, 1994). Using morphological and electrophysiological experiments combined with optogenetics, we demonstrate that cortico-pallidal synapses are effective and specific for post-synaptic GP cell types. We discuss the potential roles of cortico-pallidal projections in relation to other basal ganglia nuclei.

Results

Motor cortex innervates the GP.

We observed cortical axon collaterals in the GP using conventional tracers (BDA or PHA-L; Fig. 1A, 1C; Fig. 1-figure supplement. 1) or adenoassociated virus (AAV) vectors (Fig. 2A, 5A; Fig. 1-figure supplement 2), as reported previously (Naito & Kita, 1994).

Cortico-pallidal axon collaterals were exclusively ipsilateral (Fig. 1-figure supplement 2), implying that the layer 5 (L5) pyramidal tract (PT) type of neuron could be providing this input, thereby conveying a copy of cortical motor signals. Cortical axons were differentially distributed in the GP depending on the cortical area of origin. M1 and M2 axons were observed across the broad extent of the medio-lateral axis (range: M/L 2.4–3.7 mm; see also Fig. 1-figure supplement 1). Axon collaterals issued from the main axons and often elongated along the dorso-ventral axis (Fig. 1A, Fig. 1-figure supplement 1). Combining with immunofluorescent staining for calbindin D-28k (CB), motor cortical axons, especially from M1, were preferentially found in CB-negative [CB(-)] subregions of the GP (Fig. 1A, Fig. 1-figure supplement 1).

These axons frequently formed small sized axonal boutons (Fig. 1C, 1D). We compared the density of cortical axonal boutons in the GP, STN, and striatum. The number of boutons was greater in the striatum than in the GP or STN (Fig. 1-figure supplement 3). Since the size and efficacy of the tracer labeling were not uniform across animals, the bouton density in the GP was normalized to that in the striatum or STN for each injection. Using this normalization, the bouton density in the striatum was found to be significantly higher than in the GP ($p = 2.9\times10^{-6}$ for M1 and $p = 2.6\times10^{-6}$ for M2 using one-way ANOVA followed by Tukey test) or STN ($p = 0.0018$ for M1; $p = 0.0003$ for M2; see also Fig. 1-figure supplement 3). Bouton densities in the GP and STN were not significantly different (Fig. 1E; $p = 0.155$ using one-way ANOVA). GP bouton density did not significantly differ between M1 and M2 axons ($p = 0.32$).

These data suggested that M1 and M2 can affect the GP as strongly as they affect the STN. However, because bouton density does not directly indicate synaptic efficacy, we evaluated the electrophysiological features of cortico-pallidal projections.

Cortico-GP terminals elicit monosynaptic EPSCs.

To confirm that the observed cortico-pallidal innervation was electrophysiologically functional, we conducted whole-cell patch clamp recordings combined with optogenetic stimulation of cortical terminals using *in vitro* slice preparations. Channel rhodopsin 2 (ChR2) was introduced into cortical neurons using *AAV-hSyn-H134R-mCherry* injection into either M1 or M2 (Fig. 2A). In voltage clamp

mode at a holding potential of -60 mV, stimulation with a brief light pulse (5 ms, 470 nm) elicited inward currents in GP neurons (Fig. 2B1). The response was stable over repetitive stimulation (10 pulses at 2–10 Hz; Fig. 2B1). In current clamp mode, photoactivation elicited action potentials, although the action potential probability was affected by the spontaneous oscillation of the membrane potential (Fig. 2B2). To confirm that the photoactivated current that elicited action potentials was within the physiological range, we measured the minimum current required to induce action potentials (rheobase current) in GP neurons using 5-ms depolarizing pulses (Fig. 2C, inset). In half of GP neurons, the rheobase was less than 30 pA, and most GP neurons could emit an action potential with less than 100 pA of depolarization (N = 100 neurons; Fig. 2C). A depolarized membrane potential and a high input resistance (Table 1) led to easy induction of action potentials by small excitation.

Not all GP neurons exhibited inward photocurrent. 67/159 and 151/248 neurons did so for M1 and M2 stimulation, respectively (Fig. 2D). The locations of the GP neurons in which inward currents were observed were plotted (Fig. 2E). Consistent with the distribution of cortical axons, these locations were frequently around the center of the GP in coronal slices. Responsive neurons were similarly concentrated around the center of the GP along the rostro-caudal axis. Neurons responding to M1 terminal stimulation tended to be located in the dorsal GP, whereas those responding to M2 terminal stimulation were clustered in the ventral GP (Fig. 2E).

It is possible that the observed EPSCs were elicited by the STN via a di-synaptic circuit.

However, we used coronal slices with an anteroposterior position of 0.6 mm rostral (r0.6) – 2.2 mm caudal (c2.2) to bregma, which did not include the STN (Paxinos & Watson, 2007). Bath application of the sodium channel blocker tetrodotoxin (TTX) at 1 μM completely prevented inward currents (Fig. 3A). Additional application of the potassium channel blocker 4-aminopyridine (4AP) at 1 mM recovered the currents to up to 60% of control on average (Fig. 3A), indicating that the current was monosynaptic (Gradinaru, Mogri, Thompson, Henderson, & Deisseroth, 2009; Shu, Yu, Yang, & McCormick, 2007). Moreover, a $GABA_A$ receptor antagonist (gabazine, 20 μM) did not block the current (Fig. 3A); conversely, glutamate receptor antagonists (CNQX, 10 μM and AP-5, 20 μM) almost completely abolished the current (Fig. 3A). Thus, the inward current was mediated by glutamatergic excitatory postsynaptic currents (EPSCs). The latency (delay) of current onset after the photic stimulus in GP neurons did not differ from that in STN neurons (Fig. 3B1, 3B2). The 20–80% rise time and decay constant tended to be longer in GP neurons than in STN neurons (Fig. 3B3, 3B4). Taken together, these results indicated that the inward current observed in GP neurons was a monosynaptic, glutamatergic EPSC directly elicited by cortical terminals. Hereinafter, we refer to this current as an optically evoked EPSC (oEPSC).

M1 and M2 preferentially innervate GP neurons projecting to the striatum than those projecting to STN.

The results shown in Fig. 2C raised the question whether GP neurons have cell-type specific

cortical innervation. To determine whether cortical innervation depends on the GP-neuron projection type, we conducted *in vitro* whole cell recordings from retrogradely labeled GP_{STN} or GP_{CPu} neurons. Occasionally, we recorded large GP neurons with no or very little spontaneous activity ($N = 6$, 1.20 ± 1.79 Hz during on-cell recording mode), which possessed a distinct action potential shape. Based on earlier reports (Bengtson & Osborne, 2000; Hernandez et al., 2015), these were most likely cholinergic neurons and were excluded from subsequent analysis, although they were found to be innervated by the cortex ($N = 5/6$). In addition to the molecular profiles, the electrophysiological properties of GP_{CPu} and GP_{STN} neurons also differed. GP_{STN} neurons usually showed spontaneous repetitive firing (~20 Hz; Table 1), whereas many GP_{CPu} neurons were silent. Firing frequencies induced by depolarizing current pulses were higher in GP_{STN} than in GP_{CPu} neurons, and spike width was narrower in GP_{STN} neurons (Fig. 4B; see Table 1 for other electrophysiological parameters and quantitative comparisons). We discovered that GP_{CPu} neurons were more frequently innervated by motor cortex (51/62) than were GP_{STN} neurons (53/126). The oEPSC amplitude was also larger in GP_{CPu} neurons (Fig. 4D, E, F). The distribution of oEPSC amplitudes recorded from GP_{CPu} neurons seemed bimodal; the smaller-amplitude group was similar to GP_{STN} neurons (Fig. 4D). For comparison, MSNs ($N = 11$) and STN neurons ($N = 18$) were recorded. One-way ANOVA followed by post-hoc Tukey test revealed that the oEPSC amplitude was significantly larger in MSNs than in STN or GP neurons (for all combinations of comparisons, $p < 9\times10^{-7}$). The oEPSC amplitude of STN neurons was not significantly different from that of GP_{STN} ($p = 0.109$) or GP_{CPu} neurons ($p = 0.999$).

GP_{CPu} neurons exhibited significantly greater amplitudes than did GP_{STN} neurons (p = 0.0021; Fig. 4D). Despite the larger EPSCs, we observed relatively hyperpolarized membrane potentials and lower membrane input resistances in MSNs compared with GP or STN neurons. The mean membrane potential (V_{mean}) = -73.45 ± 5.3 mV and input resistance (R_{in}) = 79.17 ± 28.38 MΩ for 10 MSNs; V_{mean} = -45.43 ± 7.47 mV and R_{in} = 253.14 ± 156.31 MΩ for 15 STN neurons; see Table 1 for GP neurons). Thus, the ease of induction of action potentials was lower in MSNs than in GP or STN neurons, at least in slice preparation. Actually, the median of rheobase current was 695 pA for MSNs (N = 10; range. 450–1415 pA), whereas 55 pA for STN neurons (N = 30; range, 10–545 pA) and 30 pA for GP neurons (N = 100; range, 5–250 pA).

GP_{CPu} neurons were frequently innervated by either M1 (28/35) or M2 (23/27). In contrast, only a small fraction of GP_{STN} neurons received M1 (17/51) or M2 (36/75) inputs (Fig. 4C). The amplitude of M1-induced oEPSCs in the GP_{CPu} neurons was significantly larger than in the GP_{STN} neurons ($p = 1.5\times10^{-6}$ using the Wilcoxon rank sum test). This was also the case for M2-induced oEPSCs (p = 0.0038). Therefore, both motor areas preferentially innervated GP_{CPu} neurons, although GP_{STN} was more effectively innervated by M2 (Fig. 4C, 4F). Indeed, the mean oEPSC amplitude in GP_{STN} was larger with M2 stimulation than with M1 stimulation (p = 0.0028), but no significant difference between cortical sites was observed in GP_{CPu} neurons (p = 0.9595). M2 stimulation frequently evoked oEPSCs with initially smaller amplitudes, especially for the first light pulse, although repetitive light pulses at 10 Hz often augmented the oEPSC amplitude, similar to M1

279 stimulation. The paired-pulse ratio for second-to-first oEPSC in GP_{STN} neurons was 1.27 ± 0.81 for
280 M2 stimulation (N = 38) and 1.45 ± 1.20 for M1 stimulation (N = 14); in the GP_{CPu} neurons, it was
281 1.25 ± 0.62 for M2 stimulation and 1.31 ± 0.79 for M1 stimulation.

282 To further identify characteristics of GP neuron types, using retrograde labeling of GP neurons
283 and immunofluorescence against parvalbumin (PV), LIM homeobox 6 (Lhx6), and forkhead box
284 protein 2 (FoxP2), we examined molecular profiles of GP neuron projection types in Wistar rats
285 (Fujiyama, Nakano, et al., 2015). We confirmed that GP_{CPu} neurons frequently expressed FoxP2 or
286 Lhx6, but not PV (N = 659 GP_{CPu} neurons in three sections from three rats; Fig. 5), in agreement
287 with previous studies in mice (Dodson et al., 2015; Hernandez et al., 2015; Mastro et al., 2014;
288 Mizutani, Takahashi, Okamoto, Karube, & Fujiyama, 2017), Long-Evans rats (Oh et al., 2017), and
289 Sprague-Dawley rats (Abdi et al., 2015; H. Kita & Kita, 2001). The expression of FoxP2 and Lhx6
290 was almost mutually exclusive. Most PV(+) GP_{CPu} neurons co-expressed Lhx6. GP_{STN} neurons
291 lacked expression of FoxP2 but expressed PV and/or Lhx6 (N = 727 GP_{STN} neurons in three sections
292 from three rats; Fig. 5). Triple immunofluorescence combined with a single retrograde tracer
293 injection into the striatum was conducted to further elucidate the molecular identity of GP_{CPu} neurons.
294 The expression of Lhx6 (333/665) or FoxP2 (328/665) was again almost mutually exclusive. Only a
295 small fraction (14.7%) of Lhx6-expressing neurons co-expressed PV (49/333) (Fig. 5B).
296 Occasionally, double-retrogradely labeled neurons, namely bi-directional projecting GP neurons
297 (GP_{Bi}), were observed (N = 113). Lhx6 was expressed in most GP_{Bi} neurons (61/69), PV less

298 frequently (19/72), and FoxP2 rarely (2/85). GP_{Bi} neurons that expressed PV co-expressed Lhx6 in
299 most cases examined (5/6). Therefore, GP_{STN} neurons comprised PV(+) and/or Lhx6(+) prototypic
300 neurons, whereas GP_{CPu} neurons comprised arkypallidal neurons expressing FoxP2 and prototypic
301 neurons expressing Lhx6.(Fujiyama, Nakano, et al., 2015; Mallet et al., 2012). Importantly, these
302 data insist that selective electrophysiological recording from Lhx6(+) neurons can be accomplished
303 by targeting GP_{Bi} neurons. As a result, we found that GP_{Bi} also received cortical inputs (7/10 for M1
304 and 7/9 for M2; N = 3 rats for each), and most of them exhibited an oEPSCs with small amplitude
305 (Fig. 5C). Actually, the frequency distributions of oEPSC amplitudes significantly differ between
306 GP_{Bi} and GP_{CPu} neurons (Fig. 5D; $p = 2.2 \times 10^{-16}$ by the Kolmogorov-Smirnov test). It suggests that
307 arkypallidal neurons, which do not send axons to the STN, could be a principle target of
308 cortico-pallidal innervation.
309
310 ***M1 and M2 differentially innervate striatal subregions.***
311 The preceding results suggest that the two cortical motor areas project differentially to the GP. In
312 rodents, cortical pyramidal cells send axon collaterals to multiple nuclei of the BG which, in turn, are
313 themselves interconnected. Thus, M1 and M2 projections to nuclei other than the GP should involve
314 information processing in cortico-basal ganglia circuitry (Lerner et al., 2015). To quantify the
315 cortical axon distribution onto striatal molecular subregions, we employed AAV vector injection into
316 the motor area followed by immunostaining for either CB, or μ-opioid receptor (MOR) which is a

marker of the striosomes (Crittenden & Graybiel, 2011; Kincaid & Wilson, 1996; J. B. Smith et al., 2016). CB was preferentially expressed in the medial and ventral portion of the striatum and faintly in the dorsolateral striatum (Fig. 1-figure supplement 1) (H. Kita & Kita, 2001; Wouterlood, Hartig, Groenewegen, & Voorn, 2012). M1 axons were mostly confined to CB(-) subregions of the striatum (Fig. 6A), whereas M2 axons innervated both CB(-) and CB(+) striatal subregions (Fig. 6B). We quantified the axon distribution in CB(+) and CB(-) striatal subregions for both M1 and M2 axons (N = 3 rats for each subregion; 12 sections for M1 and 13 sections for M2). The proportion of CB(+) pixels that contained axons was calculated in the striatum. M2 axons were found in 37.2 ± 9.0% of CB(+) pixels, and M1 axons were found in only 15.3 ± 7.6% of CB(+) pixels (p = 0.000012 by Wilcoxon rank sum test; Fig. 6C1). To evaluate the relative strengths of the innervation, the brightness of the fluorescence in each pixel in the regions of interest (ROIs) were measured. The median pixel intensity in CB(-) ROIs was normalized to that of CB(+) ROIs. As shown in Fig. 6C2, the normalized fluorescence intensity in CB(-) striatum was ~1.6-times higher for both M1 (1.61 ± 0.39) and M2 (1.56 ± 0.28) axons. These results indicated that M2 axons innervated CB(+) striatum more frequently than did M1 axons, although CB(-) ROIs were more densely innervated by both M1 and M2 than were CB(+) ROIs.

Comparing the data in Fig. 6A and 6B shows that M1 and M2 axons exhibited differing innervation of the striosome. Based on MOR immunofluorescence, M1 axons appeared to preferentially innervate the matrix, and axon labeling in the striosomes was faint (Fig. 6D). In

contrast, M2 axons were almost equally distributed in both the striosome and matrix (Fig. 6E), as previously reported for mouse (J. B. Smith et al., 2016). We also observed topographical differences in striosome preference. In medial sections (M/L ≤ 2.9 mm), the striosomes in the ventral part of the dorsal striatum were not densely innervated by M2 axons (arrowheads in Fig. 6E2; see also Fig. 1-figure supplement 1). We quantified relative preference by normalizing fluorescence intensity in the matrix to that of the striosomes (Fig. 6F). For M2, the matrix preference was only 1.17 ± 0.22 (N = 3 rats, 126 ROIs) in lateral sections (M/L > 2.9 mm). In contrast, the matrix preference for M1 was 1.45 ± 0.26 (N = 3 rats, 155 ROIs), a significantly greater preference for the matrix than that of M2 axons ($p < 2.2\times10^{-16}$ by Wilcoxon rank sum test; Fig. 6F1). In medial sections (M/L ≤ 2.9 mm), both M1 and M2 preferred the matrix similarly, i.e., 1.37 ± 0.20 for M1 (N = 60 ROIs) and 1.36 ± 0.31 for M2 (N = 106 ROIs; Fig. 6F1). Taken together, these results show that striosomes in the dorsal striatum were selectively innervated by M2, especially in the lateral striatum.

Cortico-subthalamic (STN) projections from frontal cortical areas

Cortico-STN projections are topographically organized depending on cortical area of origin, especially in primates (Haynes & Haber, 2013; Nambu, Takada, Inase, & Tokuno, 1996; Nambu, Tokuno, Inase, & Takada, 1997). Retrograde tracer injection into the STN labeled L5 cortical neurons in a wide range of areas, among them, many neurons were found in M1, M2, and the lateral orbitofrontal area (LO) in the frontal cortex (Fig. 7-figure supplement 1). We also observed that M1

and M2 had different topographies of cortico-STN projection. M1 axons were concentrated in the central part of the STN along the anteroposterior and dorsoventral axis (Fig. 7A, B). The density of M1 axons was low around the rostral and caudal STN. The axon distribution in STN was similar between rostral and caudal M1 areas (Fig. 7A, B). Conversely, M2 axons were densely distributed in the dorso-anterior and ventro-posterior portions of the STN (Fig. 7C). LO provided dense axonal input to the rostral part of the STN (Fig. 7D). We quantified the preferential axon distribution in STN along the anteroposterior (Fig. 7E1) and dorsoventral axes (Fig. 7E2). Significant differences were observed among M1, M2, and LO ($p < 0.05$ by the Kruskal-Wallis test followed by multiple comparisons based on the Fisher Exact test with a Bonferroni correction for multiple comparisons). Of note, the topographic distribution was not clearly segregated; rather, a substantial overlap of axons from different frontal cortical areas was observed (Fig. 7F).

Neural projections among the striatum, GP, and STN

L5 PT-type neurons, candidates for the origin of the cortico-pallidal innervation, are known to project to multiple brain nuclei including the striatum and STN (T. Kita & Kita, 2012; Shepherd, 2013; Shibata et al., 2018) This suggests that when the GP receives cortical excitation, the striatum and STN are co-excited by the same source. Therefore, to elucidate the functional relevance of cortico-pallidal pathways, it is important to examine the relationship between their axon distribution and that of other, related intra-basal ganglia projections to elucidate functional relevance of

cortico-pallidal pathways. For bi-directional projections between GP and the striatum, CB expressions in the GP and striatum are correlated, such that the CB(+) striatum (medio-ventral striatum) projects to the outer edges of the GP, where CB immunoreactivity is obvious due to innervation by CB(+) striatal axon terminals (H. Kita & Kita, 2001). In contrast, the dorsolateral striatum which has sparse CB expression, innervates the central part of the GP, which lacks CB immunoreactivity (H. Kita & Kita, 2001; Rajakumar, Elisevich, & Flumerfelt, 1994; Rajakumar, Rushlow, Naus, Elisevich, & Flumerfelt, 1994). We confirmed these findings using tracer injections into the striatum (Fujiyama et al., 2011; Kawaguchi, Wilson, & Emson, 1990; Wu, Richard, & Parent, 2000) (Fig. 8). Thus, the central GP can receive direct cortical excitation (Fig. 1, 2; Fig. 1-figure supplement 1) and iMSN innervation from the dorsolateral striatum, where motor cortex preferentially projected (Fig. 6). It suggests convergence of motor cortical information. Projections from the GP to the striatum are likely to obey the same rule (Fig. 8). For GP-to-STN projections, we found topographic projection patterns as shown in Fig. 9. The rostral GP, expressing CB, projected to the rostral part of STN, whereas the central GP, lacking CB expression, projected to the central part of STN. Because the rostral STN received M2 projection and the central STN received M1 projection, again, motor cortical information can converge in the STN subregions.

Discussion

To summarize, we here report that direct motor cortical innervation of GP neurons is as dense as that of STN neurons. Pallidostriatal neurons were more frequently and heavily innervated by the cortex than were pallidosubthalamic neurons. We also investigated the distribution of cortical projections onto basal ganglia subregions, which likely affects the functions of the cortico-pallidal pathway, as discussed subsequently (see Fig. 10 for the schematic). To date, fast excitation observed in GP following cortical stimulation has been considered disynaptic excitation via the STN (Nambu et al., 2000). This does not fully contradict the present findings, since a larger population of GP neurons, GP_{STN} (or prototypic neurons), was not the main target of the motor cortex. In addition, it is possible that traditional extracellular unit recordings are biased towards neurons with relatively higher firing frequency, which include GP_{STN} neurons (Table 1). A question that remains is whether cortico-pallidal projections exist in primates including humans, as suggested (Milardi et al., 2015; Y. Smith & Wichmann, 2015).

Innervation of the basal ganglia by the frontal cortex

Topographic cortical projections are well established for the striatum and STN (Heilbronner, Meyer, Choi, & Haber, 2018; Hooks et al., 2018; Janssen et al., 2017; Mathai & Smith, 2011; Nambu, 2011; J. B. Smith et al., 2016). We also demonstrated topographic differentiation of cortico-striatal projections between M1 and M2 with distinct molecular-subdomain preferences (Fig. 6). For other frontal or associative areas, we observed that LO innervated the ventromedial part of the striatum

412 with preference for the striosomes, whereas the cingulate cortex (Cg) projected to the dorsomedial
413 striatum and avoided the striosomes, consistent with an earlier report (Friedman et al., 2015). For
414 cortico-STN projections, M1 and M2 projected densely to the central-to-caudal portions of the STN,
415 whereas LO and Cg projected to the rostromedial and caudomedial STN, respectively
416 (Supplementary Fig. 1, 2). Cortico-pallidal projections were also topographically organized; M1 and
417 M2 axons were densely distributed in the CB(-) central part of the GP (Fig. 1-figure supplement 1).
418 Cg axons projected to the GP in a similar manner. In contrast, LO provided fewer pallidal collaterals
419 (Fig. 1, Supplementary Fig. 1, 2). Thus, each frontal cortical area likely has its own regions of
420 interest in each BG nucleus. In addition, CB(-) GP was interconnected with CB(-) striatum (Fig. 8;
421 Fujiyama et al., 2011; H. Kita & Kita, 2001), and projected to the central part of the STN (Fig. 9),
422 which received projections from motor cortices, especially M1. Similar topographic interconnections
423 between STN and GP have been reported in primates (Shink, Bevan, Bolam, & Smith, 1996) and
424 rodents (Baufreton et al., 2009; but see also Canteras, Shammah-Lagnado, Silva, & Ricardo, 1990;
425 van Dijk et al., 2016). Moreover, thalamic inputs also differentiate between CB(+) and CB(-) GP (Y.
426 Smith, Raju, Pare, & Sidibe, 2004), and GP neurons form topographic pallido-pallidal connections
427 dependent on the location of the cell bodies (Sadek, Magill, & Bolam, 2007). Therefore, topographic
428 interconnections among the cortex-striatum-GP-STN likely contribute to differential integration of
429 neural signals.
430

Possible effects of cortical innervation in GP

Our findings may explain the heterogeneous activity of GP neurons during movement (Arkadir, Morris, Vaadia, & Bergman, 2004; DeLong, 1971; Dodson et al., 2015; Goldberg & Bergman, 2011; Mink & Thach, 1991a, 1991b; Turner & Anderson, 1997). The firing phases of prototypic neurons (GP_{STN}) and arkypallidal neurons corresponding to FoxP2(+) GP_{CPu} differ with regard to cortical activity (Abdi et al., 2015; Mallet et al., 2012; Mallet et al., 2016). This may be due to biased cortical innervation of GP_{CPu} (Fig. 4C, D, E, F). The axon terminal density of cortico-pallidal projections was sparser than cortico-striatal ones, but as dense as cortico-subthalamic ones. The neural connection in the basal ganglia is usually sparse; for example, even in the connection between STN and GP, which is clearly functional, only 1–2% of all GP neurons converge onto a single STN neuron and vice versa (Baufreton et al., 2009; Goldberg & Bergman, 2011). Moreover, even if excitatory synaptic inputs did not reach action potential threshold, the timing of subsequent action potentials is still altered (Ermentrout, 1996; Schultheiss, Edgerton, & Jaeger, 2010). Expression of sodium channels characteristic of GP neurons can boost excitatory synaptic inputs (Edgerton, Hanson, Gunay, & Jaeger, 2010; Hanson, Smith, & Jaeger, 2004). Thus, the relatively sparse cortical innervation to the GP_{STN} neurons could nevertheless affect a small but specific component of the basal ganglia circuitry.

Most neighboring GP neuron pairs do not exhibit real correlation (Bar-Gad, Heimer, Ritov, & Bergman, 2003; Goldberg & Bergman, 2011; Stanford, 2003), even for pause periods (Elias et al.,

2007). Excitatory inputs may synchronize GP neurons more effectively, as GP neurons tend to align with STN inputs rather than with striatal inputs (Goldberg, Kats, & Jaeger, 2003). Cortico-pallidal inputs probably precede STN-GP inputs and thus strengthen STN-GP coupling (Bevan, Magill, Hallworth, Bolam, & Wilson, 2002; Bevan, Magill, Terman, Bolam, & Wilson, 2002; Parent & Hazrati, 1995b), thereby affecting the oscillatory phase and synchronization of GP neurons.

Potential roles of the cortico-pallidal pathway

Mallet et al. (2012) reported that both MSNs and interneurons are innervated by arkypallidal neurons. Npas1(+) neurons, which overlap with Lhx6(+) and FoxP2(+) GP_{CPu} neurons, synapse onto iMSNs and dMSNs. The average inhibitory postsynaptic current amplitude is significantly larger in iMSNs (Glajch et al., 2016). In turn, iMSNs inhibit all GP neuron types equally (Hernandez et al., 2015). GP_{STN} is also activated by M2 terminals. A substantial difference among GP_{STN} cell types has been reported for innervation of the SNc (Mastro et al., 2014; Oh et al., 2017). Based on our results suggesting that M2 but not M1 project to the dorsolateral striosomes (Fig. 6) and the fact that striosomal dMSNs innervate the SNc (Fujiyama et al., 2011; Gerfen, 1985), M2-driven pathways may modulate dopamine signaling via the striatum and GP_{STN}. Recently, Viana-Magno et al. (Viana Magno et al., 2019) revealed that M2 activation can relieve the motor dysfunction of Parkinson's disease in mice. The neural circuitry proposed here is highly likely to contribute to such an effect.

As shown in Fig. 1-figure supplement 2, the cortico-pallidal pathway likely originates from PT

neurons, which also issue axon collaterals to STN (Shepherd, 2013; Shibata et al., 2018). In addition, dense labeling of L5 neurons following injection of retrograde tracer in STN (Fig. 7-figure supplement 1) suggested that STN-projecting neurons are unlikely to form a specific population of PT neurons in rodents (Shibata et al., 2018). Thus, once M1 activates, cortical signals are transmitted to the striatum, STN, and GP (Fig. 10). Due to their membrane properties, STN and GP neurons will be activated more effectively and earlier than striatal neurons (Jaeger & Kita, 2011). Since GP_{CPu} neurons are activated by direct M1 inputs, they may exhibit more activity than GP_{STN} neurons and be more in phase with cortical excitation. In contrast, GP_{STN} neurons are not strongly activated by M1. The M1-pallidal pathway therefore is unlikely to counteract hyperdirect inputs onto STN neurons. Because the latency and strength of oEPSCs in GP_{CPu} neurons were almost equal to those in STN neurons (Fig. 6, 11), STN and GP neurons may be excited simultaneously. Inhibition of MSNs by GP_{CPu} could counteract corticostriatal excitation and weaken iMSN activity. Decreased iMSN activity may reduce inhibition of GP neurons, thereby augmenting the inhibition of STN, EP, and SNr. Operation of this trisynaptic circuit may require a long duration; thus, the M1 cortico-pallidal pathway may act as a delayed terminator of the hyperdirect pathway. GP_{CPu} can also inhibit dMSNs, which in turn disinhibit the EP/SNr. If iMSN activity is suppressed by GP_{CPu}, what controls cortico-GP_{CPu} excitation? The most parsimonious explanation is that decreased cortico-pallidal activity can weaken GP excitation. In addition, GP_{CPu} inputs onto iMSNs will not completely block cortico-striatal excitation, but may delay it. It is noteworthy that striatal neurons receive contralateral

cortical excitation as well as ipsilateral input (Wilson, 1986, 1987), whereas the GP and STN receive only ipsilateral excitation (Fig. 1-figure supplement 2). It is also possible that axon collaterals of dMSNs inhibit the GP (Fujiyama et al., 2011; Kawaguchi et al., 1990; Lévesque, Bédard, Cossette, & Parent, 2003; Wu et al., 2000). In addition, pallidostriatal inhibition of striatal interneurons can possibly disinhibit MSN activity. Finally, via local boutons of GP neurons (Fujiyama, Nakano, et al., 2015; Mallet et al., 2012), mutual inhibition (Bugaysen, Bar-Gad, & Korngreen, 2013; Mastro et al., 2017; Sadek et al., 2007) may work to terminate transient excitation of the GP.

In the case of M2 input to GP, the GP_{STN} pathway can also be activated, as well as the GP_{CPu} pathway described above (Fig. 10B). M2-GP_{STN} circuitry may be more sensitive to timing, because the GP and STN form bidirectional connections, and the cortico-pallidal pathway can act as fast as the hyperdirect pathway. These two pathways may compete: if GP_{STN} is activated first, it will suppress STN; if STN is activated first, GP will be excited directly by the cortex and via the STN, in turn inhibiting the STN. Taken together, the results suggest that the net effect of M2-GP_{STN} pathway activity is likely to be suppression of the STN. However, basal ganglia activity may be strongly affected by competition between M2-pallidal and hyperdirect pathways. Because the hyperdirect pathway contributes to cessation of ongoing actions, the cortico-pallidal pathway may cancel this cessation signal. Mallet et al. (2015) proposed a two-step model for cancellation via cooperation between the STN and GP, especially arkypallidal neurons. Our current findings shed light on the linking of complex stop/cancel sequences.

Functional differentiation between M1 and M2

The overall effect of cortico-pallidal innervation may be suppression of the hyperdirect pathway, and its timing and efficacy related to the selective cortical innervation of GP cell-type(s). Therefore, our first assumption concerning the origin of the cortico-pallidal pathway should be revisited here. A paper reported that PT neurons issuing axon collaterals in the STN did not provide collaterals to the GP (T. Kita & Kita, 2012). If the hyperdirect and cortico-pallidal pathways originate from distinct neurons, the timing of activity will be substantially affected.

The findings of recent *in vivo* experiments in rodents are contradictory regarding the presence of functional differentiation between M1 and M2 during movement tasks, implying task-dependency (Makino, Hwang, Hedrick, & Komiyama, 2016). On one hand, M2 contributes to the preparatory function (Svoboda & Li, 2018), as observed in primates (Wise, 1985), or increases its influence on other cortical areas during the preparatory phase (Makino et al., 2017). PT neurons have been strongly implicated in preparatory processes as well as movement (Li et al., 2015). GP neurons are also suggested to compute action selection (Bogacz et al., 2016; Goldberg & Bergman, 2011), which likely relates to preparation of movement; and the M2-pallidal pathway may therefore contribute. It has been suggested that M2 is involved in the integration of movement with sensory or internal information (Barthas & Kwan, 2017; Saiki et al., 2014), including posture coding (Mimica, Dunn, Tombaz, Bojja, & Whitlock, 2018). It is possible that M2-GP innervation reflects sensory signal information, and contributes to the fine tuning of ongoing movement such as the adaptation of

chosen behaviors. Along with possibly involving the dopamine system, the M2-GP pathway may relate more plastic and integrated phases of movement, which may require sensitive control using two GP cell types. Natural action is a highly complex system, which involves the cerebrum, brain stem, spinal cord, and midbrain nuclei (Arber & Costa, 2018; Bostan, Dum, & Strick, 2013; Kelly & Strick, 2004). Concurrent and similar activities of M1 and M2 neurons have been reported, at least for certain movements (Saiki et al., 2014; Soma et al., 2017). Parallel connections between M1 and M2 also affect the aforementioned neural circuitry (Ueta, Hirai, Otsuka, & Kawaguchi, 2013; Ueta, Otsuka, Morishima, Ushimaru, & Kawaguchi, 2013). To conclude, the functional relevance of cortico-pallidal projections, M1/M2, and Cg differentiation for both behavioral output and neural circuitry remain to be resolved in detail.

Materials and methods

Animal experiments were approved and performed in accordance with the guidelines for the care and use of laboratory animals established by the Committee for Animal Care and Use and the Committee for Recombinant DNA Study of Doshisha University. All efforts were made to minimize animal suffering and the number of animals used.

Animal surgery for injection of neural tracers and viral vectors

Wistar SLC rats (Japan SLC Inc., Hamamatsu, Japan; N = 65 of both sexes for electrophysiological

546 experiments and *N* = 30 male rats for morphological experiments) were anesthetized with
547 intramuscular injection of a mixture of ketamine (Ketalar; Daiichi-Sankyo, Tokyo, Japan; 40 mg/kg)
548 and xylazine (Bayer HealthCare, Tokyo, Japan; 4 mg/kg). A small amount (0.05 mL) of the mixture
549 was additionally injected every 15 min during any prolonged surgery (>1 h). Body temperature was
550 monitored and controlled at 37°C with the aid of a heating device (World Precision Instruments
551 [WPI], Sarasota, FL, USA). Craniotomy was performed with a drill at an appropriate position on the
552 skull based on the rat brain atlas (Paxinos & Watson, 2007). A glass pipette (tip diameter, 30–60 μm)
553 was used for all injections. For anterograde tracers, biotinylated dextran amine (BDA, 10 kDa; 10%
554 solution dissolved in PB; Thermo Fisher Scientific, Waltham, MA, USA) was injected using either a
555 brief air pulse (10–20 psi for 40–100 ms) controlled with a coordinated valve system (PV 820, WPI)
556 or using electrophoresis (0.5–2 μA of positive current, 7 s ON/7 s OFF for 80 cycles) with a current
557 controller (WPI). PHA-L (Vector Laboratories, Burlingame, CA, USA; 2.5% dissolved in 10 mM
558 Na_2HPO_4, pH 8.0) was injected using electrophoresis (1–5 μA positive current, 7 s ON/7 s OFF for
559 80 cycles). To reduce number of rats, BDA and PHA-L were injected into different cortical areas in
560 individual rats, and brain sections derived from each rat were used for quantitative morphological
561 analysis in GP, CPu, and STN (Fig. 1, .7, Supplementary Fig. 1). AAV vectors encoding fluorophores
562 were injected using air pressure (1.5×10^{10} vg [vector genomes]/μL,
563 *AAVdj-hSyn-hChR2(H134R)-mCherry*; the plasmid a gift from Karl Deisseroth; Addgene plasmid
564 #26976; http://n2t.net/addgene:26976; RRID: Addgene_26976). For retrograde tracers, cholera toxin

565 subunit B (CTB) conjugated with Alexa Fluor 488 or 555 (Thermo Fisher Scientific) and
566 fluorophore-labeled beads (Green Retrobeads IX, LumaFluor Inc., Durham, NC, USA; FluoSphere
567 Orange 0.04 μm, Thermo Fisher Scientific) were injected using air pressure. For labeling cortical
568 neurons, injections were performed at two to three depths typically at 400 μm-intervals. The
569 stereotaxic coordinates (Paxinos & Watson, 2007) of injections in the centers of each cortical area
570 were as follows (the actual injection locations were normalized based on skull size using the distance
571 between bregma and lambda): for rostral M1, 2.0 mm rostral from bregma (A/P r2.0) and 2.5 mm
572 lateral from the midline (M/L 2.5), depth 0.5–1.2 mm from cortical surface; for caudal M1: A/P 0.0,
573 M/L 2.6, depth 0.5–1.2; for M2: A/P r4.2, M/L 1.9, depth 0.5–1.2 at a 30º angle rostral from vertical;
574 for lateral orbitofrontal area (LO): A/P r3.4, M/L 2.9, depth 4.0. Because the Cg is located at the
575 medial surface of the frontal cortex and is enclosed by M2, contamination of M2 following vertical
576 injections into the Cg would have been unavoidable. Therefore, for injections into the Cg, the
577 contralateral medial frontal area was removed using an aspiration needle and vacuum pump to
578 expose the medial surface of the frontal cortex of the targeted hemisphere. An injection electrode was
579 then inserted into the Cg at an angle of 45º (A/P r1.8, M/L 0.5) and the contents of the electrode
580 ejected into the Cg at two depths (0.5 and 1.0) using air pressure. Tracer injections into the striatum
581 were performed in two ways. To visualize striatum subregion-specific projections (Fig. 8),
582 iontophoresis was applied at a single location at A/P r1.0, M/L 3.5, depth 4.2, for injection into
583 CB-negative dorsolateral striatum, and at A/P 0.8 mm caudal to bregma (c0.8), M/L 4.0, depth 3.9

584 for CB-positive areas. For efficient retrograde labeling of GP neurons projecting to the dorsal
585 striatum, pressure injection was applied in three tracks (two depths for each track) at A/P r2.0, M/L
586 2.5, depth 3.8; A/P r1.0, M/L 3.5, depth 4.2; and A/P 0.0, M/L 3.7, depth 4.0. Micro-iontophoretic
587 injections into subregions of the GP were located at A/P c1.2 for the rostral GP, A/P c1.6 for the
588 central GP, and A/P c2.0 for the caudal GP. For these injections, the M/L and depth positions were
589 3.2 and 6.2, respectively. Tracers were injected into the STN at A/P c3.5, M/L 2.5, and depth 7.5
590 using air pressure. After injections, the skin was sutured and 2.5 mg/kg of butorphanol (Vetorphale,
591 Meiji Seika Pharma, Tokyo, Japan) was subcutaneously injected as an analgesic. The animals were
592 allowed to recover before further experimentation. We allowed 2–4 d of survival time for BDA or
593 retrograde tracers, 5–8 d for PHA-L, and 2–4 weeks for AAV. The age of rats ranged 7 to 12 weeks
594 for morphological experiments.
595
596 ***Immunohistochemistry***
597 After the survival period, rats were deeply anesthetized with an intraperitoneal injection of sodium
598 pentobarbital (100 mg/kg; Kyoritsu Seiyaku Corporation, Tokyo, Japan) and perfused with
599 pre-fixative (sucrose 8.5% w/v, $MgCl_2$ 5 mM; dissolved in 20 mM PB) followed by fixative (2 or 4%
600 paraformaldehyde and 0.2% picric acid with or without 0.05% glutaraldehyde in 0.1 M PB, pH 7.4)
601 through the cardiac artery. The brains were post-fixed *in situ* for 2–3 h, and then removed and
602 washed with PB several times. Sagittal or coronal sections 50-μm thick were cut using a vibratome

603 (Leica VT1000, Leica Instruments, Wetzlar, Germany) or freezing microtome (Leica SM 2000R),
604 and stored in PB containing 0.02% NaN_3 until further use.

605 For immunoreaction, sections were incubated with primary antibody diluted in incubation
606 buffer consisting of 10% normal goat serum, 2% bovine serum albumin, and 0.5% Triton X in 0.05
607 M Tris buffered saline (TBS) overnight at room temperature (RT) or for 2–3 d at 4°C. For
608 immunofluorescence, after rinsing with TBS three times, the sections were incubated with the
609 secondary antibodies conjugated with fluorophores for 3 h at RT. After three rinses, the sections were
610 dried on glass slides and coverslipped with antifade mounting medium (ProLong Gold, Vector). For
611 brightfield specimens, the sections were incubated with a biotinylated secondary antibody followed
612 by rinses and then reacted with ABC solution (1:200 dilution; Vector Elite) for 3 h at RT, and
613 visualized with 3,3′-diaminobenzidine (DAB), Ni-DAB or Tris-aminophenyl-methane (TAPM). The
614 sections were dehydrated with a graded series of ethanol, delipidated with xylene, and finally
615 embedded with M·X (Matsunami Glass Ind., Ltd., Osaka, Japan). The primary and secondary
616 antibodies used in this study are listed in Supplementary Tables 1 and 2.

617

618 ***Image acquisition***

619 Photomicrographs of brightfield specimens were captured using a CCD camera (DP-73, Olympus,
620 Tokyo, JAPAN) equipped with a BX-53 microscope (Olympus) using 4× (numerical aperture [N.A.]
621 0.13), 10× (N.A. 0.3), 40× (N.A. 0.75), 60× (N.A. 0.9) or 100× (N.A. 1.4; oil-immersion) objectives.

Photomicrographs were analyzed using Fiji (a distribution of Image J) (Schindelin et al., 2012), and Adobe photoshop (Adobe Systems Incorporated, Sam Jose, CA, USA). The brightness of digitized images was adjusted using the adjust-level function of these applications. To obtain a multifocus image, images were captured with 1-µm steps and processed with the "extended depth of focus" Fiji plugin. Fluorescent images were captured using an Orca Spark CMOS camera (Hamamatsu photonics, Hamamatsu, Japan) or a DP-73 camera equipped with a BX-53 microscope. To quantify the molecular expression patterns of GP neuron types, immunofluorescent images were acquired using a confocal microscope (FV1200, Olympus) with 40× (N.A. 0.95) or 100× (N.A. 1.35; silicon oil immersion) objectives.

in vitro slice recordings

Basal ganglia neurons were recorded using *in vitro* whole cell patch clamp. Rats of both sexes (N = 65; postnatal 30–65 d) were deeply anesthetized with isoflurane and perfused with 25 mL of ice-cold modified artificial cerebrospinal fluid (ACSF; N-methyl-D-glucamine, 93; KCl, 2.5; NaH_2PO_4, 1.2; $NaHCO_3$, 30; HEPES, 20; glucose, 25; sodium ascorbate, 5; thiourea, 2; sodium pyruvate, 3; $MgCl_2$, 10; and $CaCl_2$, 0.5; all in mM; pH was adjusted to 7.3 with HCl). All ACSFs were continuously aerated with 95/5% O_2/CO_2. Brains were removed and immersed in ice-cold modified ACSF for 2 min. Coronal slices 300-µm thick were cut using a vibratome (7000smz-2, Campden, Leicestershire, UK) and incubated with modified ACSF at 32°C for 15 min. The slices were transferred to normal

641 ACSF (NaCl, 125; KCl, 2.5; $CaCl_2$, 2.4; $MgCl_2$, 1.2; $NaHCO_3$, 25; glucose, 15; NaH_2PO_4, 1.25;
642 pyruvic acid, 2; lactic acid, 4; all in mM) at RT. After 1 h of recovery, slices were moved into a
643 recording chamber thermostatted at 30°C. A whole-cell glass pipette of 4–6 MΩ was filled with
644 intracellular solution (K-gluconate, 130; KCl, 2; Na_2ATP, 3; NaGTP, 0.3; $MgCl_2$, 2; Na_4EGTA, 0.6;
645 HEPES, 10; biocytin, 20.1; all in mM). The pH was adjusted to 7.3 with KOH, and the osmolality
646 was adjusted to ~290 mOsm. Target brain regions were identified with the aid of a fluorescence
647 microscope (BX-51WI, Olympus) using a ×40 water-immersed objective lens. Current clamp
648 recordings were low-pass filtered at 10 kHz and recorded using EPC10 (HEKA Elektronik Dr.
649 Schulze GmbH, Lambrecht/Pfalz, Germany) with a sampling rate of 20 kHz. The series resistance
650 was examined by applying a brief voltage pulse of -10 mV for 10 ms and was confirmed to be less
651 than 25 MΩ during recording. Shortly (less than 1 min) after achieving whole cell configuration, the
652 firing responses to 1-s depolarizing current pulses (maximum intensity was 1000 pA, increasing in
653 50-pA steps) were recorded in current clamp mode. Passive membrane properties were monitored as
654 responses to 1-s hyperpolarizing current pulses.

655 For photoactivation of ChR2, a 470-nm light-emitting diode (LED; BLS-LCS-0470-50-22,
656 Mightex Systems, Pleasanton, CA, USA) was used at full field illumination through a 40× water
657 immersion objective. Five-millisecond blue light pulses were applied at a maximum total power of
658 ~4 mW, at which neuronal responses were saturated. In some experiments, low concentrations of
659 TTX, 1 μM, and 4-amino pyridine (100 μM) were added to the ACSF to isolate monosynaptic

currents (Petreanu, Mao, Sternson, & Svoboda, 2009; Shu et al., 2007). CNQX (10 μM) and AP5 (50 μM) were applied to inhibit glutamatergic synaptic currents (N = 10), and SR95531 (gabazine; 20 μM) was applied (N = 10) to prevent $GABA_A$ receptor-mediated synaptic currents. All pharmacological reagents were purchased from Tocris Bioscience (Bristol, UK).

Slices were then fixed with a mixture of 4% paraformaldehyde, 0.05% glutaraldehyde, and 0.2% picric acid in 0.1 M PB overnight at 4°C. Fixed slices were rinsed with PB (3 × 10 min), and then re-sectioned into 50-μm-thick sections. The sections were incubated with 1% H_2O_2 in 0.05 M TBS for 30 min at RT to deplete endogenous peroxidases, then rinsed with TBS three times. The sections were incubated with CF350-conjugated streptavidin for 2 h (1:3000; Biotium, Inc., Fremont, CA) for fluorescent investigation of biocytin filled neurons. For brightfield microscopy, the sections were incubated with ABC (1:200; Elite, Vector) overnight at 4°C. Biocytin-filled neurons were visualized for light microscopy with Ni-DAB using H_2O_2 at a final concentration of 0.01%. The sections were dried on a glass slide and coverslipped with EcoMount (Biocare Medical, LLC, Concord, CA).

Data analysis

Quantification of corticostriatal axon density

To quantify the distribution of cortical axons in the striosome and matrix, regions of interest (ROI) were first set as square fields of approximately 10 × 10 pixels and located in a striosome component

679 expressing MOR. The size of the ROI was adjusted according to the size of the striosome. The
680 fluorescence intensity of each pixel in the ROI was measured, and the median was used as the
681 representative intensity for that ROI. Next, an ROI of the same size was set in the matrix close to the
682 striosome, and the median fluorescence intensity of the matrix ROI was obtained. Each striosome
683 ROI was accompanied by one matrix ROI. During ROI placement, areas containing axon bundles of
684 passage were excluded. To reduce the variance of the injection size and number of labeled neurons,
685 the fluorescence intensity of the matrix ROI was normalized to that of the striosome ROI. Thus, if
686 axons were equally distributed in the striosome and matrix, the normalized intensity would be 1.0. To
687 quantify axon density in CB-positive striatum, images of CB immunofluorescence were binarized,
688 and the number of pixels containing cortical axons were counted. The median value of pixel intensity
689 was used for representing projection strength.
690
691 ***Quantification of cortico-pallidal axon density***
692 Many thick cortical axon bundles with strong fluorescence passed through the GP, which largely
693 disrupted proportional relationships between fluorescence intensity and axon varicosity (or bouton)
694 density. Therefore, we manually counted axonal varicosities in each ROI using brightfield
695 microscopic images. ROIs of 233 × 173 μm were selected as the locations of densest axon terminals.
696 Because cortical boutons were observed in the striatum and STN of the same animal, these were also
697 counted, and the resultant bouton density was compared with those of the GP to decrease the effect

of variability of tracer injections.

Tracing and quantification of labeled cortical or pallidal axons in the STN

Axons in serial sagittal sections were manually traced on paper using a drawing tube equipped with a microscope (OPTIPHOT, Nikon Instech Co., Ltd, Tokyo, Japan) with a ×40 objective (N.A. 0.7). The tracings were scanned and saved as digital data. The resolution of a digitized image was 0.48 µm/px. For quantification using Fiji, the digitized data were converted into a binary image and the presence of axons was determined pixelwise. For comparisons of spatial axon distributions in the STN among cortical areas of origin, the STN was divided into 10 equal parts along the A/P axis or into six equal parts along the dorsoventral axis. In each division, the numbers of pixels with and without cortical axons were counted, and the proportion of axon-containing pixels to all pixels was calculated for each division. The proportion data was also normalized to the maximum value for each injection. The mean values of 2 M/L plane sections (M/L, 2.3 mm and 2.7 mm) are indicated in Fig. 7E (N = 3 rats for M1, N = 2 for M2, and N = 2 for LO).

Analysis of electrophysiological data

Our analysis method has been previously described (Mizutani et al., 2017; Oh et al., 2017). Briefly, slice recording data were analyzed using Igor Pro 7 (Wave metrics Inc., Portland, OR) with the aid of the Neuromatic plugin (http://www.neuromatic.thinkrandom.com)(Rothman & Silver, 2018) and

717 handmade procedures. Neurons in the striatum, basal nucleus of Meynert, and GP possessed distinct
718 firing properties and were readily distinguished. In the GP, GABAergic projection neurons and
719 putative cholinergic neurons were distinguishable by cell morphology and firing properties. Putative
720 cholinergic neurons were excluded from the present data. The locations of recorded cells were
721 visualized with biocytin and manually plotted on a digital image.

722

723 ***Statistical comparisons***

724 Averaged data are provided as mean ± standard deviation unless otherwise noted. Data comparison
725 among more than two groups was performed using one-way ANOVA followed by a post hoc Tukey
726 test, using R software (http://www.r-project.org/; R Project for Statistical Computing, Vienna,
727 Austria). Data comparison between two groups was performed using the Wilcoxon rank sum test. For
728 comparison of proportion values, Fisher's exact test was used. For comparison of cumulative
729 histograms, the Kolmogorov-Smirnov test was applied. Differences in data values were considered
730 significant if $p < 0.05$. Significant differences are indicated using asterisks (*, $p < 0.05$; **, $p < 0.01$;
731 ***, $p < 0.001$). All p-values are reported.

732

733

734 **Table 1.**

735 Electrophysiological properties of globus pallidus (GP) neurons

	GP_{STN} (N =108)	GP_{CPu} (N = 65)	p value
Mean membrane potential (mV)	-46.63 ± 4.95 (-34.2– -61.53)	-46.36 ± 5.9 (-33.59– -60.53)	0.682
Input resistance (MΩ)	232.35 ± 131.87 (33.1–887.45)	329.97 ± 168.19 (32.8–828.3)	6.8×10^{-05} ***
Time constant (ms)	12.94 ± 10.23 (2.25–79.75)	21.92 ± 13.11 (2.42–55.67)	2.1×10^{-07} ***
Sag potential (mV)	7.23 ± 4.52 (1.25–22.02)	8.71 ± 7 (0.63–35.18)	0.3432
Spike frequency at 100 pA depolarization (Hz)	48.46 ± 22.94 (0–103)	35.81 ± 19.6 (2–85)	0.00041 ***
Spike frequency at 500 pA depolarization (Hz)	99.14 ± 66.87 (1–244)	35.24 ± 39.24 (1–172)	1.8×10^{-09} ***
Maximum spike frequency (Hz)	135.04 ± 65.42 (11–263)	72.14 ± 36.12 (2–172)	1.0×10^{-09} ***
Current at maximum spike frequency (pA)	578.63 ± 277.97 (50–1000)	345.24 ± 219 (50–1000)	6.9×10^{-08} ***

Spike height (mV)	74.06 ± 9.77 (47.04–96.98)	76.55 ± 11.69 (38.84–95.97)	0.051
Spike width (ms)	0.95 ± 0.29 (0.63–2.29)	1.19 ± 0.32 0.7–2.17	1.6×10^{-09} ***
Spike threshold (mV)	-37.57 ± 4.79 (-24.09– -48.11)	-37.7 ± 5.32 (-23.14– -46.03)	0.5351
fAHP amplitude (mV)	21.16 ± 5.14 (9.1–38.72)	18.09 ± 4.57 (11.88–36.34)	1.3×10^{-05} ***
fAHP delay after spike peak (ms)	0.98 ± 0.39 (0.55–2.7)	1.31 ± 0.55 (0.6–3.8)	3.4×10^{-07}***
sAHP amplitude (mV)	18.26 ± 4.2 (9.47–32.87)	16.54 ± 4.71 (10.38–29.78)	0.0035 **
sAHP delay after spike peak (ms)	9.63 ± 3.32 (2.25–16.95)	22.58 ± 13.54 (2.25–65.5)	4.5×10^{-12} ***
On cell mode spontaneous firing frequency (Hz)	20.79 ± 18.74 (0–90.53)	5.47 ± 9.22 (0–35.68)	1.2×10^{-08} ***
Whole cell mode spontaneous firing frequency (Hz)	19.02 ± 13.74 (0–61.74)	9.41 ± 9.44 (0–31.85)	4.0×10^{-06} ***

736 GP_{STN}, GP neurons projecting to the subthalamic nucleus; GP_{CPu}, GP neurons projecting to the
737 striatum; fAHP, fast afterhyperpolarization; sAHP, slow afterhyperpolarization; **, $p < 0.01$; ***, p
738 < 0.001. Statistical significance was examined using the Wilcoxon rank sum test. The range of each
739 parameter is shown in parentheses.
740

References

Abdi, A., Mallet, N., Mohamed, F. Y., Sharott, A., Dodson, P. D., Nakamura, K. C., . . . Magill, P. J. (2015). Prototypic and arkypallidal neurons in the dopamine-intact external globus pallidus. *J Neurosci, 35*(17), 6667-6688. doi:10.1523/JNEUROSCI.4662-14.2015

Abrahao, K. P., & Lovinger, D. M. (2018). Classification of GABAergic neuron subtypes from the globus pallidus using wild-type and transgenic mice. *J Physiol, 596*(17), 4219-4235. doi:10.1113/JP276079

Albin, R. L., Young, A. B., & Penney, J. B. (1989). The functional anatomy of basal ganglia disorders. *Trends Neurosci, 12*(10), 366-375.

Alexander, G. E., DeLong, M. R., & Strick, P. L. (1986). Parallel organization of functionally segregated circuits linking basal ganglia and cortex. *Annu Rev Neurosci, 9*, 357-381. doi:10.1146/annurev.ne.09.030186.002041

Arber, S., & Costa, R. M. (2018). Connecting neuronal circuits for movement. *Science, 360*(6396), 1403-1404. doi:10.1126/science.aat5994

Arkadir, D., Morris, G., Vaadia, E., & Bergman, H. (2004). Independent coding of movement direction and reward prediction by single pallidal neurons. *J Neurosci, 24*(45), 10047-10056. doi:10.1523/JNEUROSCI.2583-04.2004

Bar-Gad, I., Heimer, G., Ritov, Y., & Bergman, H. (2003). Functional correlations between neighboring neurons in the primate globus pallidus are weak or nonexistent. *J Neurosci, 23*(10), 4012-4016.

Barth, T. M., Jones, T. A., & Schallert, T. (1990). Functional subdivisions of the rat somatic sensorimotor cortex. *Behav Brain Res, 39*(1), 73-95.

Barthas, F., & Kwan, A. C. (2017). Secondary Motor Cortex: Where 'Sensory' Meets 'Motor' in the Rodent Frontal Cortex. *Trends Neurosci, 40*(3), 181-193. doi:10.1016/j.tins.2016.11.006

Baufreton, J., Garret, M., Rivera, A., de la Calle, A., Gonon, F., Dufy, B., . . . Taupignon, A. (2003). D5 (not D1) dopamine receptors potentiate burst-firing in neurons of the subthalamic nucleus by modulating an L-type calcium conductance. *J Neurosci, 23*(3), 816-825.

Baufreton, J., Kirkham, E., Atherton, J. F., Menard, A., Magill, P. J., Bolam, J. P., & Bevan, M. D. (2009). Sparse but selective and potent synaptic transmission from the globus pallidus to the subthalamic nucleus. *J Neurophysiol, 102*(1), 532-545. doi:10.1152/jn.00305.2009

Bengtson, C. P., & Osborne, P. B. (2000). Electrophysiological properties of cholinergic and noncholinergic neurons in the ventral pallidal region of the nucleus basalis in rat brain slices. *J Neurophysiol, 83*(5), 2649-2660. doi:10.1152/jn.2000.83.5.2649

Bevan, M. D., Magill, P. J., Hallworth, N. E., Bolam, J. P., & Wilson, C. J. (2002). Regulation of the timing and pattern of action potential generation in rat subthalamic neurons in vitro by GABA-A IPSPs. *J Neurophysiol, 87*(3), 1348-1362.

Bevan, M. D., Magill, P. J., Terman, D., Bolam, J. P., & Wilson, C. J. (2002). Move to the rhythm: oscillations in the subthalamic nucleus-external globus pallidus network. *Trends Neurosci, 25*(10), 525-531.

779 Bissonette, G. B., Powell, E. M., & Roesch, M. R. (2013). Neural structures underlying set-shifting: roles of
780 medial prefrontal cortex and anterior cingulate cortex. *Behav Brain Res, 250*, 91-101.
781 doi:10.1016/j.bbr.2013.04.037
782 Bogacz, R., Martin Moraud, E., Abdi, A., Magill, P. J., & Baufreton, J. (2016). Properties of Neurons in
783 External Globus Pallidus Can Support Optimal Action Selection. *PLoS Comput Biol, 12*(7),
784 e1005004. doi:10.1371/journal.pcbi.1005004
785 Bolam, J. P., Hanley, J. J., Booth, P. A., & Bevan, M. D. (2000). Synaptic organisation of the basal ganglia.
786 *J Anat, 196 (Pt 4)*, 527-542.
787 Bostan, A. C., Dum, R. P., & Strick, P. L. (2013). Cerebellar networks with the cerebral cortex and basal
788 ganglia. *Trends Cogn Sci, 17*(5), 241-254. doi:10.1016/j.tics.2013.03.003
789 Brown, A. R., & Teskey, G. C. (2014). Motor cortex is functionally organized as a set of spatially distinct
790 representations for complex movements. *J Neurosci, 34*(41), 13574-13585.
791 doi:10.1523/JNEUROSCI.2500-14.2014
792 Bugaysen, J., Bar-Gad, I., & Korngreen, A. (2013). Continuous modulation of action potential firing by a
793 unitary GABAergic connection in the globus pallidus in vitro. *J Neurosci, 33*(31), 12805-12809.
794 doi:10.1523/JNEUROSCI.1970-13.2013
795 Calabresi, P., Picconi, B., Tozzi, A., Ghiglieri, V., & Di Filippo, M. (2014). Direct and indirect pathways of
796 basal ganglia: a critical reappraisal. *Nat Neurosci, 17*(8), 1022-1030. doi:10.1038/nn.3743
797 Canteras, N. S., Shammah-Lagnado, S. J., Silva, B. A., & Ricardo, J. A. (1990). Afferent connections of the
798 subthalamic nucleus: a combined retrograde and anterograde horseradish peroxidase study in the
799 rat. *Brain Res, 513*(1), 43-59.
800 Cao, V. Y., Ye, Y., Mastwal, S., Ren, M., Coon, M., Liu, Q., . . . Wang, K. H. (2015). Motor Learning
801 Consolidates Arc-Expressing Neuronal Ensembles in Secondary Motor Cortex. *Neuron, 86*(6),
802 1385-1392. doi:10.1016/j.neuron.2015.05.022
803 Cooper, A. J., & Stanford, I. M. (2000). Electrophysiological and morphological characteristics of three
804 subtypes of rat globus pallidus neurone in vitro. *J Physiol, 527 Pt 2*, 291-304.
805 Crittenden, J. R., & Graybiel, A. M. (2011). Basal Ganglia disorders associated with imbalances in the
806 striatal striosome and matrix compartments. *Front Neuroanat, 5*, 59.
807 doi:10.3389/fnana.2011.00059
808 Cui, G., Jun, S. B., Jin, X., Pham, M. D., Vogel, S. S., Lovinger, D. M., & Costa, R. M. (2013). Concurrent
809 activation of striatal direct and indirect pathways during action initiation. *Nature, 494*(7436),
810 238-242. doi:10.1038/nature11846
811 DeLong, M. R. (1971). Activity of pallidal neurons during movement. *J Neurophysiol, 34*(3), 414-427.
812 doi:10.1152/jn.1971.34.3.414
813 DeLong, M. R. (1990). Primate models of movement disorders of basal ganglia origin. *Trends Neurosci, 13*,
814 281-285.
815 Dodson, P. D., Larvin, J. T., Duffell, J. M., Garas, F. N., Doig, N. M., Kessaris, N., . . . Magill, P. J. (2015).
816 Distinct developmental origins manifest in the specialized encoding of movement by adult

817 neurons of the external globus pallidus. *Neuron, 86*(2), 501-513. doi:10.1016/j.neuron.2015.03.007
818 Ebbesen, C. L., Insanally, M. N., Kopec, C. D., Murakami, M., Saiki, A., & Erlich, J. C. (2018). More than
819 Just a "Motor": Recent Surprises from the Frontal Cortex. *J Neurosci, 38*(44), 9402-9413.
820 doi:10.1523/JNEUROSCI.1671-18.2018
821 Eblen, F., & Graybiel, A. M. (1995). Highly restricted origin of prefrontal cortical inputs to striosomes in
822 the macaque monkey. *J Neurosci, 15*(9), 5999-6013.
823 Ebrahimi, A., Pochet, R., & Roger, M. (1992). Topographical organization of the projections from
824 physiologically identified areas of the motor cortex to the striatum in the rat. *Neurosci Res, 14*(1),
825 39-60.
826 Edgerton, J. R., Hanson, J. E., Gunay, C., & Jaeger, D. (2010). Dendritic sodium channels regulate
827 network integration in globus pallidus neurons: a modeling study. *J Neurosci, 30*(45),
828 15146-15159. doi:10.1523/JNEUROSCI.2662-10.2010
829 Elias, S., Joshua, M., Goldberg, J. A., Heimer, G., Arkadir, D., Morris, G., & Bergman, H. (2007).
830 Statistical properties of pauses of the high-frequency discharge neurons in the external segment
831 of the globus pallidus. *J Neurosci, 27*(10), 2525-2538. doi:10.1523/JNEUROSCI.4156-06.2007
832 Ermentrout, B. (1996). Type I membranes, phase resetting curves, and synchrony. *Neural Comput, 8*(5),
833 979-1001.
834 Frank, M. J., Samanta, J., Moustafa, A. A., & Sherman, S. J. (2007). Hold your horses: impulsivity, deep
835 brain stimulation, and medication in parkinsonism. *Science, 318*(5854), 1309-1312.
836 doi:10.1126/science.1146157
837 Friedman, A., Homma, D., Gibb, L. G., Amemori, K., Rubin, S. J., Hood, A. S., . . . Graybiel, A. M. (2015). A
838 Corticostriatal Path Targeting Striosomes Controls Decision-Making under Conflict. *Cell, 161*(6),
839 1320-1333. doi:10.1016/j.cell.2015.04.049
840 Friend, D. M., & Kravitz, A. V. (2014). Working together: basal ganglia pathways in action selection.
841 *Trends Neurosci, 37*(6), 301-303. doi:10.1016/j.tins.2014.04.004
842 Fujiyama, F., Nakano, T., Matsuda, W., Furuta, T., Udagawa, J., & Kaneko, T. (2015). A single-neuron
843 tracing study of arkypallidal and prototypic neurons in healthy rats. *Brain Struct Funct*.
844 doi:10.1007/s00429-015-1152-2
845 Fujiyama, F., Sohn, J., Nakano, T., Furuta, T., Nakamura, K. C., Matsuda, W., & Kaneko, T. (2011).
846 Exclusive and common targets of neostriatofugal projections of rat striosome neurons: a single
847 neuron-tracing study using a viral vector. *Eur J Neurosci, 33*(4), 668-677.
848 doi:10.1111/j.1460-9568.2010.07564.x
849 Fujiyama, F., Takahashi, S., & Karube, F. (2015). Morphological elucidation of basal ganglia circuits
850 contributing reward prediction. *Front Neurosci, 9*, 6. doi:10.3389/fnins.2015.00006
851 Fujiyama, F., Unzai, T., Nakamura, K., Nomura, S., & Kaneko, T. (2006). Difference in organization of
852 corticostriatal and thalamostriatal synapses between patch and matrix compartments of rat
853 neostriatum. *Eur J Neurosci, 24*(10), 2813-2824. doi:10.1111/j.1460-9568.2006.05177.x
854 Gabbott, P. L., Warner, T. A., Jays, P. R., Salway, P., & Busby, S. J. (2005). Prefrontal cortex in the rat:

projections to subcortical autonomic, motor, and limbic centers. *J Comp Neurol, 492*(2), 145-177. doi:10.1002/cne.20738

Gerfen, C. R. (1985). The neostriatal mosaic. I. Compartmental organization of projections from the striatum to the substantia nigra in the rat. *J Comp Neurol, 236*(4), 454-476. doi:10.1002/cne.902360404

Gittis, A. H., Berke, J. D., Bevan, M. D., Chan, C. S., Mallet, N., Morrow, M. M., & Schmidt, R. (2014). New roles for the external globus pallidus in basal ganglia circuits and behavior. *J Neurosci, 34*(46), 15178-15183. doi:10.1523/JNEUROSCI.3252-14.2014

Glajch, K. E., Kelver, D. A., Hegeman, D. J., Cui, Q., Xenias, H. S., Augustine, E. C., . . . Chan, C. S. (2016). Npas1+ Pallidal Neurons Target Striatal Projection Neurons. *J Neurosci, 36*(20), 5472-5488. doi:10.1523/JNEUROSCI.1720-15.2016

Goldberg, J. A., & Bergman, H. (2011). Computational physiology of the neural networks of the primate globus pallidus: function and dysfunction. *Neuroscience, 198*, 171-192. doi:10.1016/j.neuroscience.2011.08.068

Goldberg, J. A., Kats, S. S., & Jaeger, D. (2003). Globus pallidus discharge is coincident with striatal activity during global slow wave activity in the rat. *J Neurosci, 23*(31), 10058-10063. doi:10.1523/JNEUROSCI.23-31-10058.2003

Gradinaru, V., Mogri, M., Thompson, K. R., Henderson, J. M., & Deisseroth, K. (2009). Optical deconstruction of parkinsonian neural circuitry. *Science, 324*(5925), 354-359. doi:10.1126/science.1167093

Guo, Z. V., Li, N., Huber, D., Ophir, E., Gutnisky, D., Ting, J. T., . . . Svoboda, K. (2014). Flow of cortical activity underlying a tactile decision in mice. *Neuron, 81*(1), 179-194. doi:10.1016/j.neuron.2013.10.020

Hanson, J. E., Smith, Y., & Jaeger, D. (2004). Sodium channels and dendritic spike initiation at excitatory synapses in globus pallidus neurons. *J Neurosci, 24*(2), 329-340. doi:10.1523/JNEUROSCI.3937-03.2004

Haynes, W. I., & Haber, S. N. (2013). The organization of prefrontal-subthalamic inputs in primates provides an anatomical substrate for both functional specificity and integration: implications for Basal Ganglia models and deep brain stimulation. *J Neurosci, 33*(11), 4804-4814. doi:10.1523/JNEUROSCI.4674-12.2013

Hegeman, D. J., Hong, E. S., Hernandez, V. M., & Chan, C. S. (2016). The external globus pallidus: progress and perspectives. *Eur J Neurosci, 43*(10), 1239-1265. doi:10.1111/ejn.13196

Heilbronner, S. R., Meyer, M. A. A., Choi, E. Y., & Haber, S. N. (2018). How do cortico-striatal projections impact on downstream pallidal circuitry? *Brain Struct Funct, 223*(6), 2809-2821. doi:10.1007/s00429-018-1662-9

Heindorf, M., Arber, S., & Keller, G. B. (2018). Mouse Motor Cortex Coordinates the Behavioral Response to Unpredicted Sensory Feedback. *Neuron, 99*(5), 1040-1054 e1045. doi:10.1016/j.neuron.2018.07.046

Hernandez, V. M., Hegeman, D. J., Cui, Q., Kelver, D. A., Fiske, M. P., Glajch, K. E., . . . Chan, C. S. (2015). Parvalbumin+ Neurons and Npas1+ Neurons Are Distinct Neuron Classes in the Mouse External Globus Pallidus. *J Neurosci, 35*(34), 11830-11847. doi:10.1523/JNEUROSCI.4672-14.2015

Hikosaka, O. (2007). GABAergic output of the basal ganglia. *Prog Brain Res, 160*, 209-226.

Hintiryan, H., Foster, N. N., Bowman, I., Bay, M., Song, M. Y., Gou, L., . . . Dong, H. W. (2016). The mouse cortico-striatal projectome. *Nat Neurosci, 19*(8), 1100-1114. doi:10.1038/nn.4332

Hira, R., Ohkubo, F., Masamizu, Y., Ohkura, M., Nakai, J., Okada, T., & Matsuzaki, M. (2014). Reward-timing-dependent bidirectional modulation of cortical microcircuits during optical single-neuron operant conditioning. *Nat Commun, 5*, 5551. doi:10.1038/ncomms6551

Hira, R., Ohkubo, F., Ozawa, K., Isomura, Y., Kitamura, K., Kano, M., . . . Matsuzaki, M. (2013). Spatiotemporal dynamics of functional clusters of neurons in the mouse motor cortex during a voluntary movement. *J Neurosci, 33*(4), 1377-1390. doi:10.1523/JNEUROSCI.2550-12.2013

Hontanilla, B., Parent, A., de las Heras, S., & Gimenez-Amaya, J. M. (1998). Distribution of calbindin D-28k and parvalbumin neurons and fibers in the rat basal ganglia. *Brain Res Bull, 47*(2), 107-116.

Hooks, B. M., Papale, A. E., Paletzki, R. F., Feroze, M. W., Eastwood, B. S., Couey, J. J., . . . Gerfen, C. R. (2018). Topographic precision in sensory and motor corticostriatal projections varies across cell type and cortical area. *Nat Commun, 9*(1), 3549. doi:10.1038/s41467-018-05780-7

Hunnicutt, B. J., Jongbloets, B. C., Birdsong, W. T., Gertz, K. J., Zhong, H., & Mao, T. (2016). A comprehensive excitatory input map of the striatum reveals novel functional organization. *Elife, 5*. doi:10.7554/eLife.19103

Isoda, M., & Hikosaka, O. (2008). Role for subthalamic nucleus neurons in switching from automatic to controlled eye movement. *J Neurosci, 28*(28), 7209-7218. doi:10.1523/JNEUROSCI.0487-08.2008

Isomura, Y., Takekawa, T., Harukuni, R., Handa, T., Aizawa, H., Takada, M., & Fukai, T. (2013). Reward-modulated motor information in identified striatum neurons. *J Neurosci, 33*(25), 10209-10220. doi:10.1523/JNEUROSCI.0381-13.2013

Jaeger, D., & Kita, H. (2011). Functional connectivity and integrative properties of globus pallidus neurons. *Neuroscience, 198*, 44-53. doi:10.1016/j.neuroscience.2011.07.050

Janssen, M. L. F., Temel, Y., Delaville, C., Zwartjes, D. G. M., Heida, T., De Deurwaerdere, P., . . . Benazzouz, A. (2017). Cortico-subthalamic inputs from the motor, limbic, and associative areas in normal and dopamine-depleted rats are not fully segregated. *Brain Struct Funct, 222*(6), 2473-2485. doi:10.1007/s00429-016-1351-5

Kawaguchi, Y., Wilson, C. J., & Emson, P. C. (1990). Projection subtypes of rat neostriatal matrix cells revealed by intracellular injection of biocytin. *J Neurosci, 10*(10), 3421-3438.

Kawai, R., Markman, T., Poddar, R., Ko, R., Fantana, A. L., Dhawale, A. K., . . . Olveczky, B. P. (2015). Motor cortex is required for learning but not for executing a motor skill. *Neuron, 86*(3), 800-812. doi:10.1016/j.neuron.2015.03.024

Kelly, R. M., & Strick, P. L. (2004). Macro-architecture of basal ganglia loops with the cerebral cortex: use

of rabies virus to reveal multisynaptic circuits. *Prog Brain Res, 143*, 449-459.

Kim, H. F., Ghazizadeh, A., & Hikosaka, O. (2014). Separate groups of dopamine neurons innervate caudate head and tail encoding flexible and stable value memories. *Front Neuroanat, 8*, 120. doi:10.3389/fnana.2014.00120

Kincaid, A. E., & Wilson, C. J. (1996). Corticostriatal innervation of the patch and matrix in the rat neostriatum. *J Comp Neurol, 374*(4), 578-592. doi:10.1002/(SICI)1096-9861(19961028)374:4<578::AID-CNE7>3.0.CO;2-Z

Kita, H. (2007). Globus pallidus external segment. *Prog Brain Res, 160*, 111-133.

Kita, H., & Kita, T. (2001). Number, origins, and chemical types of rat pallidostriatal projection neurons. *J Comp Neurol, 437*(4), 438-448.

Kita, T., & Kita, H. (2012). The subthalamic nucleus is one of multiple innervation sites for long-range corticofugal axons: a single-axon tracing study in the rat. *J Neurosci, 32*(17), 5990-5999. doi:10.1523/JNEUROSCI.5717-11.2012

Lévesque, M., Bédard, A., Cossette, M., & Parent, A. (2003). Novel aspects of the chemical anatomy of the striatum and its efferents projections. *J Chem Neuroanat, 26*(4), 271-281. doi:10.1016/j.jchemneu.2003.07.001

Lerner, T. N., Shilyansky, C., Davidson, T. J., Evans, K. E., Beier, K. T., Zalocusky, K. A., . . . Deisseroth, K. (2015). Intact-Brain Analyses Reveal Distinct Information Carried by SNc Dopamine Subcircuits. *Cell, 162*(3), 635-647. doi:10.1016/j.cell.2015.07.014

Li, N., Chen, T. W., Guo, Z. V., Gerfen, C. R., & Svoboda, K. (2015). A motor cortex circuit for motor planning and movement. *Nature, 519*(7541), 51-56. doi:10.1038/nature14178

Mailly, P., Aliane, V., Groenewegen, H. J., Haber, S. N., & Deniau, J. M. (2013). The rat prefrontostriatal system analyzed in 3D: evidence for multiple interacting functional units. *J Neurosci, 33*(13), 5718-5727. doi:10.1523/JNEUROSCI.5248-12.2013

Makino, H., Hwang, E. J., Hedrick, N. G., & Komiyama, T. (2016). Circuit Mechanisms of Sensorimotor Learning. *Neuron, 92*(4), 705-721. doi:10.1016/j.neuron.2016.10.029

Makino, H., Ren, C., Liu, H., Kim, A. N., Kondapaneni, N., Liu, X., . . . Komiyama, T. (2017). Transformation of Cortex-wide Emergent Properties during Motor Learning. *Neuron, 94*(4), 880-890 e888. doi:10.1016/j.neuron.2017.04.015

Mallet, N., Micklem, B. R., Henny, P., Brown, M. T., Williams, C., Bolam, J. P., . . . Magill, P. J. (2012). Dichotomous organization of the external globus pallidus. *Neuron, 74*(6), 1075-1086. doi:10.1016/j.neuron.2012.04.027

Mallet, N., Schmidt, R., Leventhal, D., Chen, F., Amer, N., Boraud, T., & Berke, J. D. (2016). Arkypallidal Cells Send a Stop Signal to Striatum. *Neuron*. doi:10.1016/j.neuron.2015.12.017

Manita, S., Suzuki, T., Homma, C., Matsumoto, T., Odagawa, M., Yamada, K., . . . Murayama, M. (2015). A Top-Down Cortical Circuit for Accurate Sensory Perception. *Neuron, 86*(5), 1304-1316. doi:10.1016/j.neuron.2015.05.006

Mastro, K. J., Bouchard, R. S., Holt, H. A., & Gittis, A. H. (2014). Transgenic mouse lines subdivide

external segment of the globus pallidus (GPe) neurons and reveal distinct GPe output pathways. *J Neurosci, 34*(6), 2087-2099. doi:10.1523/JNEUROSCI.4646-13.2014

Mastro, K. J., Zitelli, K. T., Willard, A. M., Leblanc, K. H., Kravitz, A. V., & Gittis, A. H. (2017). Cell-specific pallidal intervention induces long-lasting motor recovery in dopamine-depleted mice. *Nat Neurosci, 20*(6), 815-823. doi:10.1038/nn.4559

Mathai, A., & Smith, Y. (2011). The corticostriatal and corticosubthalamic pathways: two entries, one target. So what? *Front Syst Neurosci, 5*, 64. doi:10.3389/fnsys.2011.00064

Matsumoto, M., & Hikosaka, O. (2009). Two types of dopamine neuron distinctly convey positive and negative motivational signals. *Nature, 459*(7248), 837-841. doi:10.1038/nature08028

Menegas, W., Bergan, J. F., Ogawa, S. K., Isogai, Y., Umadevi Venkataraju, K., Osten, P., . . . Watabe-Uchida, M. (2015). Dopamine neurons projecting to the posterior striatum form an anatomically distinct subclass. *Elife, 4*, e10032. doi:10.7554/eLife.10032

Middleton, F. A., & Strick, P. L. (2000). Basal ganglia and cerebellar loops: motor and cognitive circuits. *Brain Res Brain Res Rev, 31*(2-3), 236-250.

Middleton, F. A., & Strick, P. L. (2002). Basal-ganglia 'projections' to the prefrontal cortex of the primate. *Cereb Cortex, 12*(9), 926-935.

Milardi, D., Gaeta, M., Marino, S., Arrigo, A., Vaccarino, G., Mormina, E., . . . Quartarone, A. (2015). Basal ganglia network by constrained spherical deconvolution: a possible cortico-pallidal pathway? *Mov Disord, 30*(3), 342-349. doi:10.1002/mds.25995

Mimica, B., Dunn, B. A., Tombaz, T., Bojja, V., & Whitlock, J. R. (2018). Efficient cortical coding of 3D posture in freely behaving rats. *Science, 362*(6414), 584-589. doi:10.1126/science.aau2013

Mink, J. W., & Thach, W. T. (1991a). Basal ganglia motor control. I. Nonexclusive relation of pallidal discharge to five movement modes. *J Neurophysiol, 65*(2), 273-300. doi:10.1152/jn.1991.65.2.273

Mink, J. W., & Thach, W. T. (1991b). Basal ganglia motor control. II. Late pallidal timing relative to movement onset and inconsistent pallidal coding of movement parameters. *J Neurophysiol, 65*(2), 301-329. doi:10.1152/jn.1991.65.2.301

Miyamoto, D., Hirai, D., Fung, C. C., Inutsuka, A., Odagawa, M., Suzuki, T., . . . Murayama, M. (2016). Top-down cortical input during NREM sleep consolidates perceptual memory. *Science, 352*(6291), 1315-1318. doi:10.1126/science.aaf0902

Miyamoto, Y., & Fukuda, T. (2015). Immunohistochemical study on the neuronal diversity and three-dimensional organization of the mouse entopeduncular nucleus. *Neurosci Res, 94*, 37-49. doi:10.1016/j.neures.2015.02.006

Mizutani, K., Takahashi, S., Okamoto, S., Karube, F., & Fujiyama, F. (2017). Substance P effects exclusively on prototypic neurons in mouse globus pallidus. *Brain Struct Funct, 222*(9), 4089-4110. doi:10.1007/s00429-017-1453-8

Murakami, M., Shteingart, H., Loewenstein, Y., & Mainen, Z. F. (2017). Distinct Sources of Deterministic and Stochastic Components of Action Timing Decisions in Rodent Frontal Cortex. *Neuron, 94*(4), 908-919 e907. doi:10.1016/j.neuron.2017.04.040

1007 Murakami, M., Vicente, M. I., Costa, G. M., & Mainen, Z. F. (2014). Neural antecedents of self-initiated
1008 actions in secondary motor cortex. *Nat Neurosci, 17*(11), 1574-1582. doi:10.1038/nn.3826
1009 Nakayama, Y., Yokoyama, O., & Hoshi, E. (2015). Distinct neuronal organizations of the caudal cingulate
1010 motor area and supplementary motor area in monkeys for ipsilateral and contralateral hand
1011 movements. *J Neurophysiol, 113*(7), 2845-2858. doi:10.1152/jn.00854.2014
1012 Naito, A., & Kita, H. (1994). The cortico-pallidal projection in the rat: an anterograde tracing study with
1013 biotinylated dextran amine. *Brain Res, 653*(1-2), 251-257.
1014 Nambu, A. (2007). Globus pallidus internal segment. . *Prog Brain Res, 160*(135-150).
1015 Nambu, A. (2008). Seven problems on the basal ganglia. *Curr Opin Neurobiol, 18*(6), 595-604.
1016 doi:10.1016/j.conb.2008.11.001
1017 Nambu, A. (2011). Somatotopic organization of the primate Basal Ganglia. *Front Neuroanat, 5*, 26.
1018 doi:10.3389/fnana.2011.00026
1019 Nambu, A., Takada, M., Inase, M., & Tokuno, H. (1996). Dual somatotopical representations in the
1020 primate subthalamic nucleus: evidence for ordered but reversed body-map transformations from
1021 the primary motor cortex and the supplementary motor area. *J Neurosci, 16*(8), 2671-2683.
1022 Nambu, A., Tokuno, H., Hamada, I., Kita, H., Imanishi, M., Akazawa, T., . . . Hasegawa, N. (2000).
1023 Excitatory cortical inputs to pallidal neurons via the subthalamic nucleus in the monkey. *J*
1024 *Neurophysiol, 84*(1), 289-300.
1025 Nambu, A., Tokuno, H., Inase, M., & Takada, M. (1997). Corticosubthalamic input zones from forelimb
1026 representations of the dorsal and ventral divisions of the premotor cortex in the macaque monkey:
1027 comparison with the input zones from the primary motor cortex and the supplementary motor
1028 area. *Neurosci Lett, 239*(1), 13-16.
1029 Nambu, A., Tokuno, H., & Takada, M. (2002). Functional significance of the cortico-subthalamo-pallidal
1030 'hyperdirect' pathway. *Neurosci Res, 43*(2), 111-117.
1031 Oh, Y. M., Karube, F., Takahashi, S., Kobayashi, K., Takada, M., Uchigashima, M., . . . Fujiyama, F. (2017).
1032 Using a novel PV-Cre rat model to characterize pallidonigral cells and their terminations. *Brain*
1033 *Struct Funct, 222*(5), 2359-2378. doi:10.1007/s00429-016-1346-2
1034 Parent, A., Fortin, M., Cote, P. Y., & Cicchetti, F. (1996). Calcium-binding proteins in primate basal
1035 ganglia. *Neurosci Res, 25*(4), 309-334.
1036 Parent, A., & Hazrati, L. N. (1995a). Functional anatomy of the basal ganglia. I. The cortico-basal
1037 ganglia-thalamo-cortical loop. *Brain Res Brain Res Rev, 20*(1), 91-127.
1038 Parent, A., & Hazrati, L. N. (1995b). Functional anatomy of the basal ganglia. II. The place of subthalamic
1039 nucleus and external pallidum in basal ganglia circuitry. *Brain Res Brain Res Rev, 20*(1), 128-154.
1040 Passingham, R. E., & Wise, S. P. (2012). *The neurobiology of prefrontal cortex. Anatomy, evolution, and*
1041 *the origin of insight.* Oxford: Oxford University Press.
1042 Paus, T. (2001). Primate anterior cingulate cortex: where motor control, drive and cognition interface. *Nat*
1043 *Rev Neurosci, 2*(6), 417-424. doi:10.1038/35077500
1044 Paxinos, G., & Watson, C. (2007). *The rat brain in stereotaxic coordinates* (6th ed.). San Diego, USA:

Academic Press.

Petreanu, L., Mao, T., Sternson, S. M., & Svoboda, K. (2009). The subcellular organization of neocortical excitatory connections. *Nature, 457*(7233), 1142-1145. doi:10.1038/nature07709

Rajakumar, N., Elisevich, K., & Flumerfelt, B. A. (1994). The pallidostriatal projection in the rat: a recurrent inhibitory loop? *Brain Res, 651*(1-2), 332-336.

Rajakumar, N., Rushlow, W., Naus, C. C., Elisevich, K., & Flumerfelt, B. A. (1994). Neurochemical compartmentalization of the globus pallidus in the rat: an immunocytochemical study of calcium-binding proteins. *J Comp Neurol, 346*(3), 337-348. doi:10.1002/cne.903460303

Redgrave, P., Rodriguez, M., Smith, Y., Rodriguez-Oroz, M. C., Lehericy, S., Bergman, H., . . . Obeso, J. A. (2010). Goal-directed and habitual control in the basal ganglia: implications for Parkinson's disease. *Nat Rev Neurosci, 11*(11), 760-772. doi:10.1038/nrn2915

Reep, R. L., & Corwin, J. V. (1999). Topographic organization of the striatal and thalamic connections of rat medial agranular cortex. *Brain Res, 841*(1-2), 43-52.

Reep, R. L., Wu, J. H., Cheatwood, J. L., Corwin, J. V., Kartje, G. L., & Mir, A. (2008). Quantification of synaptic density in corticostriatal projections from rat medial agranular cortex. *Brain Res, 1233*, 27-34. doi:10.1016/j.brainres.2008.07.059

Rothman, J. S., & Silver, R. A. (2018). NeuroMatic: An Integrated Open-Source Software Toolkit for Acquisition, Analysis and Simulation of Electrophysiological Data. *Front Neuroinform, 12*, 14. doi:10.3389/fninf.2018.00014

Rouiller, E. M., Moret, V., & Liang, F. (1993). Comparison of the connectional properties of the two forelimb areas of the rat sensorimotor cortex: support for the presence of a premotor or supplementary motor cortical area. *Somatosens Mot Res, 10*(3), 269-289.

Sadek, A. R., Magill, P. J., & Bolam, J. P. (2007). A single-cell analysis of intrinsic connectivity in the rat globus pallidus. *J Neurosci, 27*(24), 6352-6362. doi:10.1523/JNEUROSCI.0953-07.2007

Saiki, A., Kimura, R., Samura, T., Fujiwara-Tsukamoto, Y., Sakai, Y., & Isomura, Y. (2014). Different modulation of common motor information in rat primary and secondary motor cortices. *PLoS One, 9*(6), e98662. doi:10.1371/journal.pone.0098662

Schindelin, J., Arganda-Carreras, I., Frise, E., Kaynig, V., Longair, M., Pietzsch, T., . . . Cardona, A. (2012). Fiji: an open-source platform for biological-image analysis. *Nat Methods, 9*(7), 676-682. doi:10.1038/nmeth.2019

Schmidt, R., Leventhal, D. K., Mallet, N., Chen, F., & Berke, J. D. (2013). Canceling actions involves a race between basal ganglia pathways. *Nat Neurosci, 16*(8), 1118-1124. doi:10.1038/nn.3456

Schoenbaum, G., Roesch, M. R., Stalnaker, T. A., & Takahashi, Y. K. (2009). A new perspective on the role of the orbitofrontal cortex in adaptive behaviour. *Nat Rev Neurosci, 10*(12), 885-892. doi:10.1038/nrn2753

Schultheiss, N. W., Edgerton, J. R., & Jaeger, D. (2010). Phase response curve analysis of a full morphological globus pallidus neuron model reveals distinct perisomatic and dendritic modes of synaptic integration. *J Neurosci, 30*(7), 2767-2782. doi:10.1523/JNEUROSCI.3959-09.2010

Shepherd, G. M. (2013). Corticostriatal connectivity and its role in disease. *Nat Rev Neurosci, 14*(4), 278-291. doi:10.1038/nrn3469

Shibata, K.-I., Tanaka, T., Hioki, H., & Furuta, T. (2018). Projection Patterns of Corticofugal Neurons Associated with Vibrissa Movement. *eNeuro, 5*(5), ENEURO.0190-0118.2018. doi:10.1523/eneuro.0190-18.2018

Shink, E., Bevan, M. D., Bolam, J. P., & Smith, Y. (1996). The subthalamic nucleus and the external pallidum: two tightly interconnected structures that control the output of the basal ganglia in the monkey. *Neuroscience, 73*(2), 335-357.

Shink, E., & Smith, Y. (1995). Differential synaptic innervation of neurons in the internal and external segments of the globus pallidus by the GABA- and glutamate-containing terminals in the squirrel monkey. *J Comp Neurol, 358*(1), 119-141. doi:10.1002/cne.903580108

Shipp, S. (2016). The functional logic of corticostriatal connections. *Brain Struct Funct*. doi:10.1007/s00429-016-1250-9

Shu, Y., Yu, Y., Yang, J., & McCormick, D. A. (2007). Selective control of cortical axonal spikes by a slowly inactivating K+ current. *Proc Natl Acad Sci U S A, 104*(27), 11453-11458. doi:10.1073/pnas.0702041104

Smith, J. B., Klug, J. R., Ross, D. L., Howard, C. D., Hollon, N. G., Ko, V. I., . . . Jin, X. (2016). Genetic-Based Dissection Unveils the Inputs and Outputs of Striatal Patch and Matrix Compartments. *Neuron, 91*(5), 1069-1084. doi:10.1016/j.neuron.2016.07.046

Smith, Y., Bevan, M. D., Shink, E., & Bolam, J. P. (1998). Microcircuitry of the direct and indirect pathways of the basal ganglia. *Neuroscience, 86*(2), 353-387.

Smith, Y., Raju, D. V., Pare, J. F., & Sidibe, M. (2004). The thalamostriatal system: a highly specific network of the basal ganglia circuitry. *Trends Neurosci, 27*(9), 520-527. doi:10.1016/j.tins.2004.07.004

Smith, Y., & Wichmann, T. (2015). The cortico-pallidal projection: an additional route for cortical regulation of the basal ganglia circuitry. *Mov Disord, 30*(3), 293-295. doi:10.1002/mds.26095

Smith, Y., Wichmann, T., & DeLong, M. R. (2014). Corticostriatal and mesocortical dopamine systems: do species differences matter? *Nat Rev Neurosci, 15*(1), 63. doi:10.1038/nrn3469-c1

Soma, S., Saiki, A., Yoshida, J., Rios, A., Kawabata, M., Sakai, Y., & Isomura, Y. (2017). Distinct Laterality in Forelimb-Movement Representations of Rat Primary and Secondary Motor Cortical Neurons with Intratelencephalic and Pyramidal Tract Projections. *J Neurosci, 37*(45), 10904-10916. doi:10.1523/JNEUROSCI.1188-17.2017

Stanford, I. M. (2003). Independent neuronal oscillators of the rat globus pallidus. *J Neurophysiol, 89*(3), 1713-1717. doi:10.1152/jn.00864.2002

Sul, J. H., Jo, S., Lee, D., & Jung, M. W. (2011). Role of rodent secondary motor cortex in value-based action selection. *Nat Neurosci, 14*(9), 1202-1208. doi:10.1038/nn.2881

Sul, J. H., Kim, H., Huh, N., Lee, D., & Jung, M. W. (2010). Distinct roles of rodent orbitofrontal and medial prefrontal cortex in decision making. *Neuron, 66*(3), 449-460.

doi:10.1016/j.neuron.2010.03.033

Svoboda, K., & Li, N. (2018). Neural mechanisms of movement planning: motor cortex and beyond. *Curr Opin Neurobiol, 49*, 33-41. doi:10.1016/j.conb.2017.10.023

Tsumori, T., Yokota, S., Kishi, T., Qin, Y., Oka, T., & Yasui, Y. (2006). Insular cortical and amygdaloid fibers are in contact with posterolateral hypothalamic neurons projecting to the nucleus of the solitary tract in the rat. *Brain Res, 1070*(1), 139-144. doi:10.1016/j.brainres.2005.11.040

Turner, R. S., & Anderson, M. E. (1997). Pallidal discharge related to the kinematics of reaching movements in two dimensions. *J Neurophysiol, 77*(3), 1051-1074. doi:10.1152/jn.1997.77.3.1051

Ueta, Y., Hirai, Y., Otsuka, T., & Kawaguchi, Y. (2013). Direction- and distance-dependent interareal connectivity of pyramidal cell subpopulations in the rat frontal cortex. *Front Neural Circuits, 7*, 164. doi:10.3389/fncir.2013.00164

Ueta, Y., Otsuka, T., Morishima, M., Ushimaru, M., & Kawaguchi, Y. (2013). Multiple Layer 5 Pyramidal Cell Subtypes Relay Cortical Feedback from Secondary to Primary Motor Areas in Rats. *Cereb Cortex*. doi:10.1093/cercor/bht088

van Dijk, K. J., Janssen, M. L., Zwartjes, D. G., Temel, Y., Visser-Vandewalle, V., Veltink, P. H., . . . Heida, T. (2016). Spatial Localization of Sources in the Rat Subthalamic Motor Region Using an Inverse Current Source Density Method. *Front Neural Circuits, 10*, 87. doi:10.3389/fncir.2016.00087

Viana Magno, L. A., Tenza-Ferrer, H., Collodetti, M., Felipe Guimaraes Aguiar, M., Paula Carneiro Rodrigues, A., Souza da Silva, R., . . . Aurelio Romano-Silva, M. (2019). Optogenetic stimulation of the M2 cortex reverts motor dysfunction in a mouse model of Parkinson's Disease. *J Neurosci*. doi:10.1523/JNEUROSCI.2277-18.2019

Vicente, A. M., Galvao-Ferreira, P., Tecuapetla, F., & Costa, R. M. (2016). Direct and indirect dorsolateral striatum pathways reinforce different action strategies. *Curr Biol, 26*(7), R267-269. doi:10.1016/j.cub.2016.02.036

Voorn, P., Vanderschuren, L. J., Groenewegen, H. J., Robbins, T. W., & Pennartz, C. M. (2004). Putting a spin on the dorsal-ventral divide of the striatum. *Trends Neurosci, 27*(8), 468-474. doi:10.1016/j.tins.2004.06.006

Wallace, M. L., Saunders, A., Huang, K. W., Philson, A. C., Goldman, M., Macosko, E. Z., . . . Sabatini, B. L. (2017). Genetically Distinct Parallel Pathways in the Entopeduncular Nucleus for Limbic and Sensorimotor Output of the Basal Ganglia. *Neuron, 94*(1), 138-152 e135. doi:10.1016/j.neuron.2017.03.017

Wei, W., & Wang, X. J. (2016). Inhibitory Control in the Cortico-Basal Ganglia-Thalamocortical Loop: Complex Regulation and Interplay with Memory and Decision Processes. *Neuron, 92*(5), 1093-1105. doi:10.1016/j.neuron.2016.10.031

Wichmann, T., & DeLong, M. R. (1996). Functional and pathophysiological models of the basal ganglia. *Curr Opin Neurobiol, 6*(6), 751-758.

Wilson, C. J. (1986). Postsynaptic potentials evoked in spiny neostriatal projection neurons by stimulation of ipsilateral and contralateral neocortex. *Brain Res, 367*(1-2), 201-213.

Wilson, C. J. (1987). Morphology and synaptic connections of crossed corticostriatal neurons in the rat. *J Comp Neurol, 263*(4), 567-580. doi:10.1002/cne.902630408

Wise, S. P. (1985). The primate premotor cortex: past, present, and preparatory. *Annu Rev Neurosci, 8*, 1-19. doi:10.1146/annurev.ne.08.030185.000245

Wouterlood, F. G., Hartig, W., Groenewegen, H. J., & Voorn, P. (2012). Density gradients of vesicular glutamate- and GABA transporter-immunoreactive boutons in calbindinand mu-opioid receptor-defined compartments in the rat striatum. *J Comp Neurol, 520*(10), 2123-2142. doi:10.1002/cne.23031

Wu, Y., Richard, S., & Parent, A. (2000). The organization of the striatal output system: a single-cell juxtacellular labeling study in the rat. *Neurosci Res, 38*(1), 49-62.

Xiao, C., Miwa, J. M., Henderson, B. J., Wang, Y., Deshpande, P., McKinney, S. L., & Lester, H. A. (2015). Nicotinic receptor subtype-selective circuit patterns in the subthalamic nucleus. *J Neurosci, 35*(9), 3734-3746. doi:10.1523/JNEUROSCI.3528-14.2015

Figure legends

Fig. 1. Motor cortical axons project to the globus pallidus (GP).

(A) A representative image of axons in the GP originated from the secondary motor cortex (M2), labeled with biotinylated dextran amine (BDA; visualized in black). Axon collaterals in the GP are predominantly distributed in the calbindin (CB)-negative subregions. CB is visualized in brown. (B) Images and drawings of BDA injection sites into the primary and secondary motor areas (M1 and M2, respectively). Tracer was deposited across the entire thickness of the cortex. (C) Images of axon distributions in the GP, striatum, and subthalamic nucleus (STN) from M1 and M2. The sections were counter-stained with an anti-parvalbumin (PV) antibody, visualized in brown. (D) Magnified views of cortical axon varicosities (arrowheads) in the GP; **left**, M1 axons; **right**, M2 axons. The images are composites from multiple focal planes, and show that the PV neurons are unlikely to be contacted by axon varicosities. (E) Comparison of axon varicosity density in GP with that in the STN and striatum (N = 3 rats). The axon varicosity density in the GP as normalized values to that in the STN (E1), or to that in the striatum (E2).

Fig. 2. Photoactivation of motor cortical terminals evokes excitation in GP neurons.

(A) Schematic (**top**) of AAV encoding channel rhodopsin 2 and mCherry injection into the motor cortex for *ex vivo* recordings using coronal slices. Examples of AAV injection sites are shown in the **middle** panels (red). Images of immunofluorescence for neurofilament 200 kDa (N200, **bottom**),

used for identification of the M1/M2 border (white dotted lines). (B1) A representative voltage clamp trace (held at -60 mV) showing inward currents in GP neurons elicited by 5-ms blue light pulses (470 nm). (B2) A representative current clamp trace showing photoinduced action potentials and excitatory postsynaptic potentials (EPSPs, arrowheads). (C) Cumulative histogram of the rheobase current of GP neurons. Note that 25 to 30 pA is sufficient to elicit action potentials in half of GP neurons (N = 100). (D) Proportion of GP neurons innervated by M1 or M2 terminals. The number of neurons is shown in bars. M2 more frequently innervated the GP than did M1. (E) Location of GP neurons innervated by M1 (red circle) or M2 (blue circle). Note the topographic distribution of M1 and M2 innervation. The size of circles represents the amplitude of optically evoked currents,

Fig. 3. Cortico-pallidal connections are monosynaptic and glutamatergic.

(A) The current induced by optogenetic stimulation of cortical terminals is monosynaptic and glutamatergic. (A1) Representative traces of pharmacological effects on the light-induced inward current. **Top**, no treatment; **Middle**, effects of TTX, 4AP, and gabazine; **Bottom**, effects of additional application of glutamate receptor antagonists (CNQX, AP5). (A2) A summary plot of pharmacological treatments (N = 10 GP neurons from 4 rats). (B) Comparison of the time courses of optogenetically evoked EPSCs (oEPSCs). (B1) Representative traces recorded from STN (black) and GP (red) neurons. The GP and STN neurons were not recorded simultaneously. (B2-4) Summary plots of oEPSC time courses in STN and GP neurons. (B2) The latency from light onset to oEPSC

onset does not differ between STN and GP neurons (both $N = 15$ neurons from 6 rats). The rise time (B3) and the decay constant (B4) of oEPSCs ($N = 15$ GP neurons and 12 STN neurons).Statistical significance was examined by the Wilcoxon rank sum test. The STN and GP neurons were recorded from the different brain slices of the same animal.

Fig. 4. Cell type-dependent cortical innervation of pallidal neurons

(A) Schematic of *ex vivo* recordings from retrogradely labeled GP neurons to investigate the effect of GP neuron projection type on cortical innervation. (B) Electrophysiological differences between GP neurons projecting to the striatum (GP_{CPu}) and STN (GP_{STN}) (see also Table 1). (C) The proportion of GP neurons innervated by M1 or M2 is correlated with projection type. GP_{CPu} neurons were more often innervated by either M1 or M2 than were GP_{STN}. Significance was examined using Fisher's exact test with a Bonferroni correction for multiple comparisons (***, $p < 0.00025$; **, $p < 0.0025$; *, $p < 0.0125$).(D) Amplitudes of oEPSCs in GP, STN, and striatal neurons. The amplitude in GP_{CPu} neurons is similar to that in STN neurons but smaller than that in striatal medium spiny neurons (MSNs). From each rat, CPu, GP and STN neurons were recorded in the same experimental session. Data obtained from M1 and M2 stimulation are summed. (E) Cumulative histograms of oEPSC amplitude in GP_{CPu} and GP_{STN} neurons. GP_{CPu} neurons exhibit a greater optically evoked EPSC (oEPSC) amplitude. (F) **Left**, amplitudes of oEPSCs induced in GP neurons by M1 terminal stimulation. The GP_{CPu} group shows larger oEPSC amplitudes than the GP_{STN} group. **Right**,

amplitudes of oEPSCs induced by M2 terminal stimulation. Significantly larger oEPSCs were again recorded in the GP_{CPu} group ($p = 0.034$), but the difference is small. The neurons represented in Fig. 4 are not the same population as shown in Fig. 2, except for in Fig. 2C.

Fig. 5. Cortical inputs on bi-directional projection GP neurons (GP_{Bi})

Two distinct retrograde tracers were injected into the STN and striatum (CPu), respectively. (A) Three combinations of double immunofluorescence (PV/Lhx6, PV/FoxP2, and Lhx6/FoxP2) were applied (N = 3. rats). CPu-projecting GP neurons (GP_{CPu}) expressed either FoxP2 or Lhx6 exclusively (A1), whereas STN-projecting GP neurons (GP_{STN}) were mainly composed of PV- and/or Lhx6- expressing neurons (A2). (A3) GP neurons projecting to both the CPu and STN (GP_{Bi}) frequently expressed Lhx6, but not FoxP2. (B) Triple immunofluorescence for GP_{CPu} neurons (N = 2. rats). Only a single retrograde tracer was injected into the striatum. (C) oEPSC amplitude of GP_{Bi} neurons (N = 3. rats for each M1 and M2 labeling). Most of GP_{Bi} exhibited small amplitude of oEPSCs. Green and red retrobeads were injected into the CPu and STN, respectively. Confocal images of a biocytin filled GP_{Bi} neuron (arrowheads) are shown. AAV-labeled cortical axons also show red fluorescence. (D) Cumulative histograms of oEPSC amplitude in GP_{Bi} and GP_{CPu} neurons. The distributions are significantly different ($p = 2.2 \times 10^{-16}$ by the Kolmogorov-Smirnov test). The histogram of GP_{CPu} neurons is the same as shown in Fig. 4E.

Fig. 6. Distribution of cortico-striatal axons in striatal subregions

(A) Distribution of M1 cortico-striatal axons (magenta) in relation to calbindin (CB) expression (green). Sagittal sections at two mediolateral (M/L) coordinates are shown (A1, M/L 3.7 mm; A2, M/L 3.2 mm). Note that M1 axons were densely distributed in the dorsolateral striatum, where CB expression was weak. (B) M2 corticostriatal axons. M2 axons were distributed in the CB(+) and dorsal CB(-) subregions at M/L 3.7 mm (B1) and M/L 3.2 mm (B2). (C) Quantitative comparison of axon distributions between M1 and M2 (for each $N = 3$ rats). (C1) Proportion of axon-containing pixels in the CB(+) striatum. M2 axons more frequently innervated the CB(+) striatum than did M1 axons. (C2) Normalized fluorescence intensity in the CB(-) striatum, which reflects axon density, was not significantly different between M1 and M2. The dotted line at 1.0 indicates axon density in the CB(+) striatum. (D) Distribution of M1 axons in the striosome/matrix subregions of the striatum. Upper panel, M1 axons (magenta) are overlaid with μ-opioid receptor (MOR) immunofluorescence (green). Dotted area in the panel is magnified in the bottom two panels. The fluorescence of M1 axons (**bottom left**) and MOR (**bottom right**) is shown in grayscale. MOR immunopositive striosomes are contoured by white dotted lines. Note that M1 axons seemingly avoided the striosomes in both lateral (D1, M/L 3.4 mm) and medial (D2, M/L 2.8 mm) sections. (E) Distribution of M2 axons in the striatum, as described in (D). Note that in lateral sections (M/L 3.4 mm, E1), M2 axons were uniformly distributed in both matrix and striosome, whereas in medial sections (M/L 2.8 mm, E2), M2 axons were observed in dorsal but not ventral striosomes (arrowheads). (F) Normalized

fluorescence intensity in the matrix (N = 3 rats for each M1 and M2 labeling). M1 axons were more densely distributed in the matrix in lateral sections (M/L > 2.9 mm, F1), whereas both M1 and M2 preferentially innervated the matrix in medial sections (M/L ≤ 2.9 mm, F2). The dotted black line represents axon density in the striosomes. The sections from the same rat were used for either CB or MOR immunostaining.

Fig. 7. Distribution of cortico-subthalamic axons

Images and drawings of BDA injection sites into rostral M1 (A1), caudal M1 (B1), M2 (C1), and lateral orbitofrontal area (LO). LO injections often extended to the insular area. However, additional experiments revealed that the insular cortex did not send many axons to the STN, as previously reported (Tsumori et al., 2006).Cortical axons in STN are represented in two sagittal planes (M/L 2.3 and 2.7 mm) for M1 (A2, B2), M2 (C2), and LO (D2). The gray dotted line indicates the boundary of the STN. (E) Normalized distribution of cortical axons in the STN along the A/P (E1) or D/V axis (E2). Data from sections M/L 2.3 mm and 2.7 mm are pooled (N = 3 rats for M1, N = 2 for M2, and N = 2 for LO). (F) Merged traces of axons from M1, M2, and LO (N = 2 rats for each cortex). M1 (black) terminated in the central part of the STN, whereas M2 axons (green) were dense in the posterior-ventral portion.

Fig. 8. Reciprocal projections between the striatum and GP

Cholera toxin subunit B conjugated with Alexa-Fluor-488 (CTB488) was injected into the striatum (CPu), either the CB(+) (A1) or CB(-) (B1) subregions. CTB488 can be transported in both anterograde and retrograde directions. In the GP, anterogradely labeled terminals of medium spiny neurons (MSNs) (arrowheads in A2 and B2) and labeled GP neurons projecting to the CPu (arrowheads in A3 and B3) were observed. Reciprocal projections between CPu and GP correlated with CB expression. Dotted lines show the boundary of the striatum (A1, B1), the GP (B2, C2), and CB(+)/CB(-) subregions of the GP (A3, B3). Representative images from one rat for each are shown.

Fig. 9. Projections from GP to STN

(A), (B), (C) **Left**, Images of BDA injection sites in the GP subregions. Sections containing the injection core (arrowheads) were counterstained for CB (magenta). Thick dotted lines indicate the borders of the GP, and thin dotted lines indicate the borders of CB(+) and CB(-) subregions of the GP. **Right**, Drawings of labeled GP axons in the STN. Labeled axons (black) in the STN were traced over STN contours (green). Rostral GP projected to rostral STN (A; N = 3 rats) and central GP to central STN (B; N = 6 rats). (C) In one case, we observed caudal GP projections to caudal STN (N = 1 rat). (D) Injection around the border between the GP and the internal capsule (N = 1 rat). Axons in the STN are uniformly distributed in the STN, probably due to labeling of fibers of passage from the entire GP. Four to eight STN sections are overlaid for each case. Scales shown in A pertain also to B and C. The labeled axons do not include striatal MSN axons because the striatum does not project to

the STN. Passing fibers of cortico-STN projections may also be labeled with tracer injections into the GP; however, this is unlikely in our experiments because the morphology of axonal boutons in the STN differed between cortical and GP injections (E), as reported in monkeys (Shink & Smith, 1995).

Fig. 10. Schematic drawings of the cortex-basal ganglia circuitry

Diagram of cortico-basal ganglia-thalamus circuitry. The dotted lines represent the relatively weak innervation reported in this study for cortex to GP_{STN}, and for GP_{CPu} to dMSNs (Glajch et al., 2016). The numbers in circles indicate estimated conduction times in millisecond (ms) (Jaeger & Kita, 2011). (A) M1 activation induces excitation in the striatum, STN, and GP_{CPu}. Due to the electrophysiological properties of the neurons, STN and GP may be activated faster than striatal neurons. (B) M2 activation conveys additional excitation to the GP_{STN} neurons. Possible information flow related to the present study is shown by red lines. Note that inhibition from the GP is here considered faster (1 ms) than excitation from the STN (2–3 ms) (Jaeger & Kita, 2011). The actual timing of spike activity depends on neuron type, and excitation/inhibition interactions are complex. (C) Schematic of connections among the basal ganglia nuclei with relation to M1 and M2 innervation.

Figure-figure supplement legends

Fig. 1-figure supplement 1. Example images of M2 projections to the striatum and GP (related to Fig. 1).

Using BDA injections into M2, labeled axons are visualized in black and CB immunoactivity in brown. Axons are densely distributed in the striatum lateral to the midline (M/L 2.1–4.3 mm). In more lateral sections, axons were denser in CB(-) subregions, and were also found in striosomes (small CB[-] subregions) throughout the entire projection field (open arrowheads). In medial sections, M2 axons were observed in both CB(+) and CB(-) subregions. M2 axons were only faintly detected in ventral striosomes (filled arrowheads), whereas they were relatively dense in dorsal striosomes (open arrowheads). Note also the presence of M2 axons in CB(-) portions of the GP (arrows).

Fig. 1-figure supplement 2. Cortico-pallidal projections are restricted to the ipsilateral hemisphere (related to Fig. 1).

Representative images of AAV-labeled cortical axons in the basal ganglia originating in M2, in both hemispheres. **Left**, M2 axons were observed in the ipsilateral GP (**upper**) and STN (**lower**). In contrast, no fluorescent signal was observed in contralateral GP (**upper**) or STN (**lower**). The images in the contralateral hemisphere were captured with high exposures to better visualize brain structures, because no fluorescent signal was detected there. GP, globus pallidus; STN subthalamic nucleus; ic, internal capsule.

Fig. 1-figure supplement 3. Number of cortical boutons in the striatum, STN, and GP originating from M1, M2, and LO (related to Fig. 1, also related to Fig. 5 and Supplementary Fig. 1).

Fig. 7-figure supplement 1. Representative distribution of STN-projecting cortical neurons (related to Fig. 5).

(A) **Left**, retrogradely labeled cortical neurons projecting to the STN. Note that many L5A neurons were labeled in the frontal cortical area. **Right**, calbindin (CB) immunofluorescence (green) in the same section. Cortical layers are indicated with Roman numerals. (B) Plots of STN-projecting cortical neurons (black dots). Most labeled neurons are located in the frontal area including AI (the anterior insular area), the Cg (cingulate area), the LO (lateral orbitofrontal area), M1 (primary motor area), M2 (secondary motor area), and the VO (ventral orbitofrontal area). Some neurons are also located in S1 (primary somatosensory area) and the RSD (retrosplenial dysgranular area). (C) CTB555 was injected into the STN. ic, internal capsule; ZI, zona incerta. The effects of faint tracer leak to cortex and thalamus are considered negligible because very few labeled neurons are observed in L2/3 or L6, respectively.

Karube et al. 2019 Fig.1

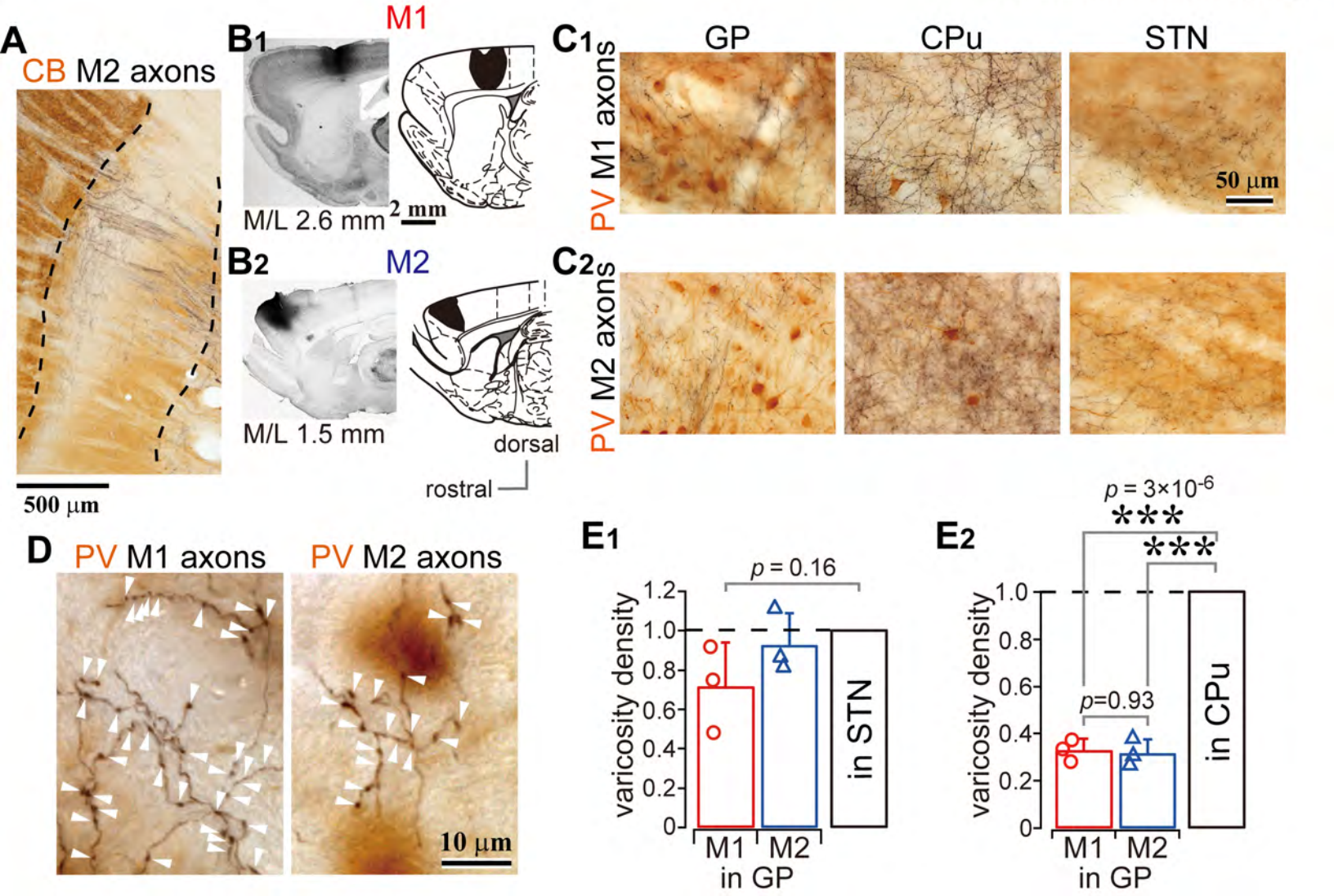

Karube et al,. 2019 Fig.2

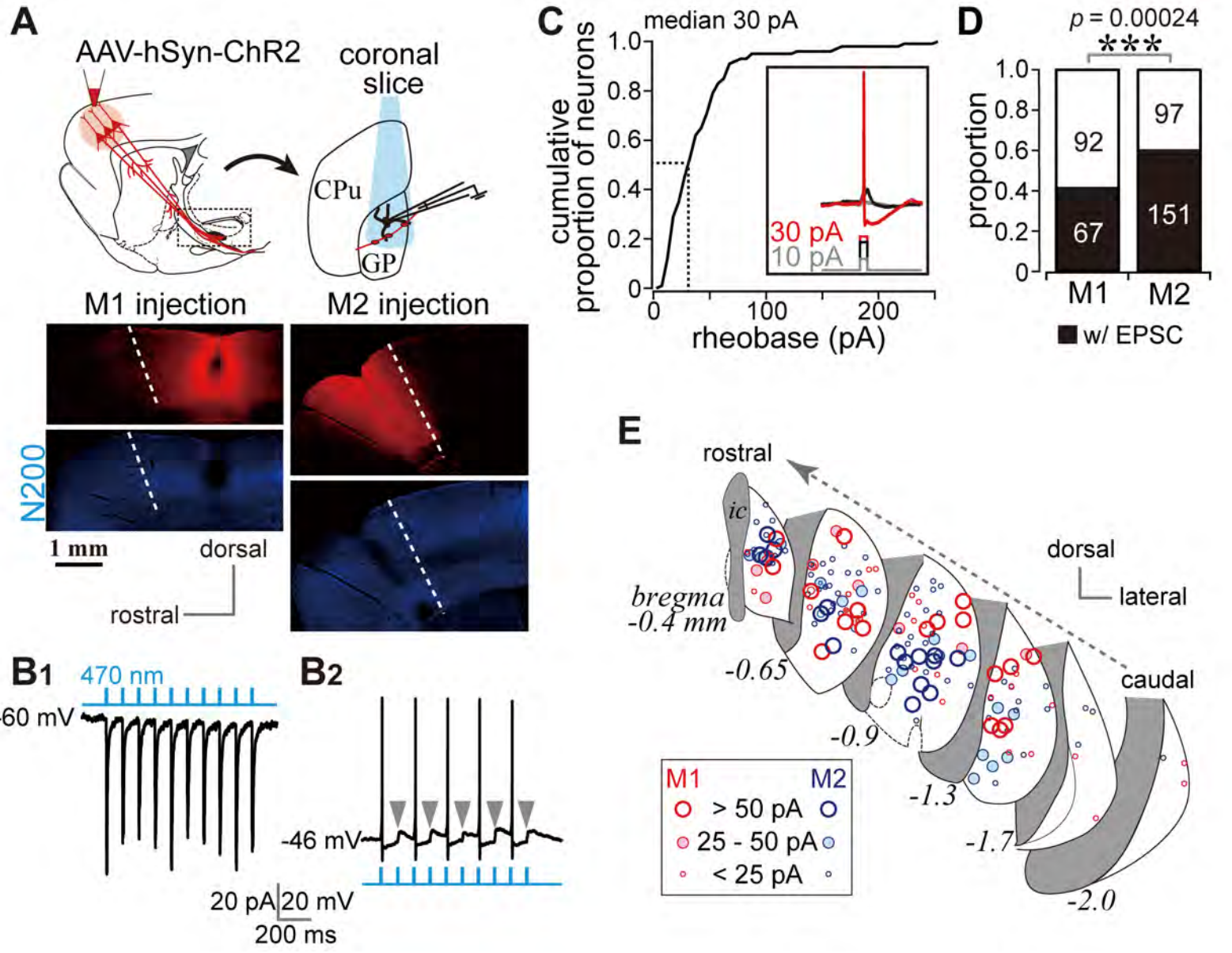

Karube et al. 2019 Fig.3

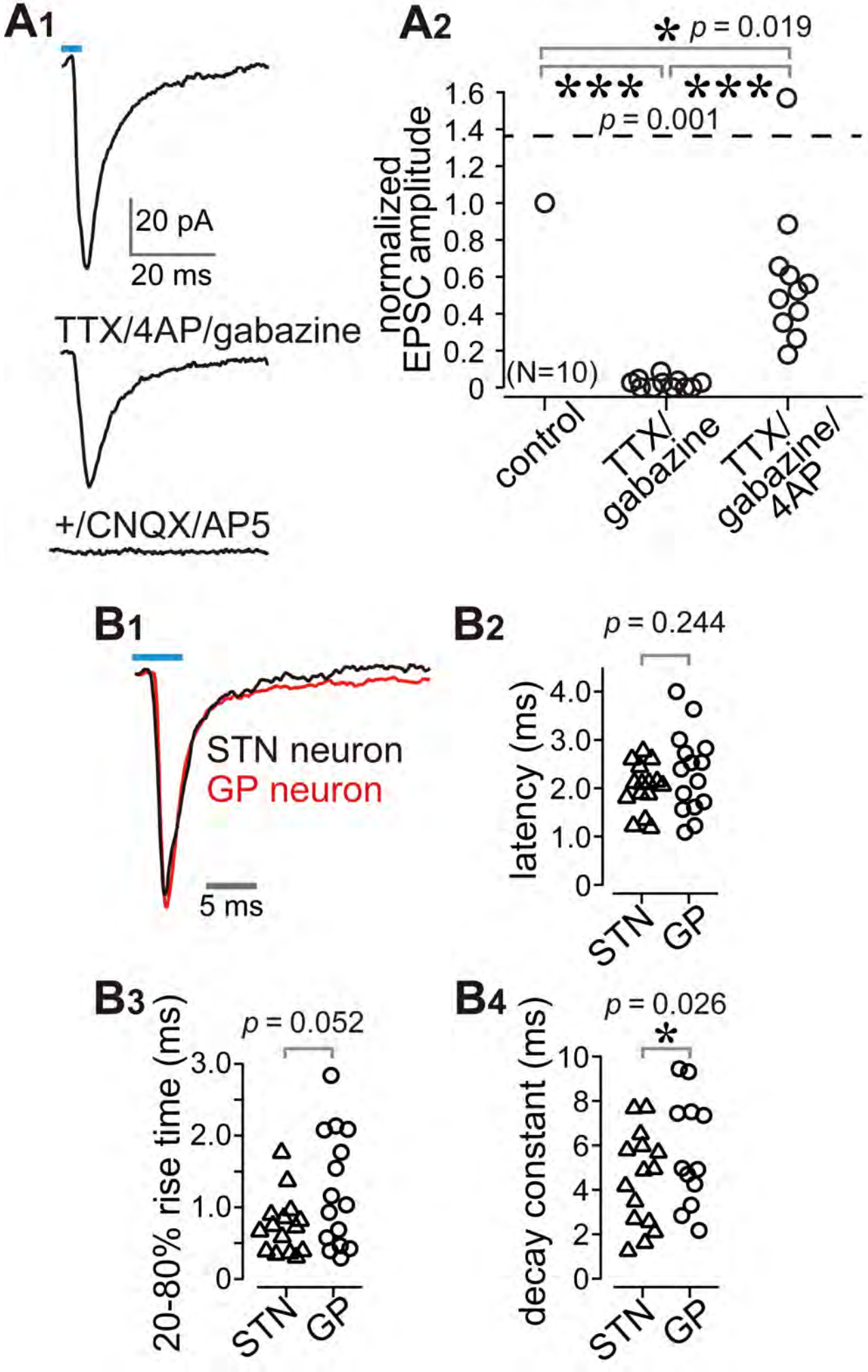

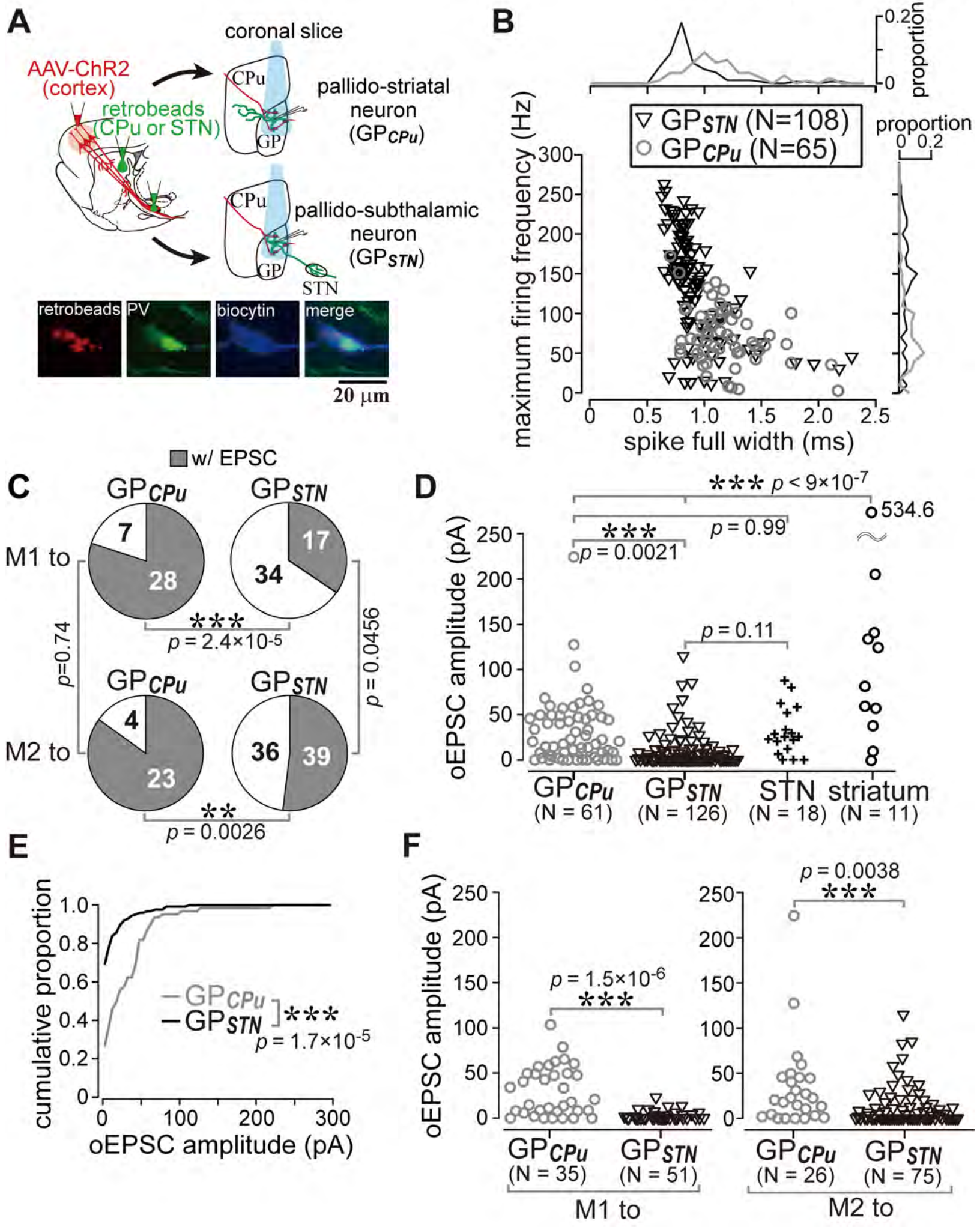
A
coronal slice
AAV-ChR2
(cortex)
retrobeads
(CPu or STN)
CPu
GP
pallido-striatal
neuron
(GP$_{CPu}$)
pallido-subthalamic
neuron
(GP$_{STN}$)
STN
retrobeads
PV
biocytin
merge
20 μm
B
proportion
0.2
0
GP$_{STN}$ (N=108)
GP$_{CPu}$ (N=65)
maximum firing frequency (Hz)
spike full width (ms)
C
w/ EPSC
GP$_{CPu}$
GP$_{STN}$
M1 to
M2 to
7
28
17
34
4
23
36
39
***
p = 2.4×10-5
p=0.74
p = 0.0456
**
p = 0.0026
D
*** p < 9×10-7
***
p = 0.0021
p = 0.99
p = 0.11
534.6
oEPSC amplitude (pA)
GP$_{CPu}$ (N = 61)
GP$_{STN}$ (N = 126)
STN (N = 18)
striatum (N = 11)
E
cumulative proportion
GP$_{CPu}$
GP$_{STN}$
***
p = 1.7×10-5
oEPSC amplitude (pA)
F
p = 1.5×10-6
***
p = 0.0038
***
oEPSC amplitude (pA)
GP$_{CPu}$ (N = 35)
GP$_{STN}$ (N = 51)
GP$_{CPu}$ (N = 26)
GP$_{STN}$ (N = 75)
M1 to
M2 to

Karube et al. 2019 Fig.5

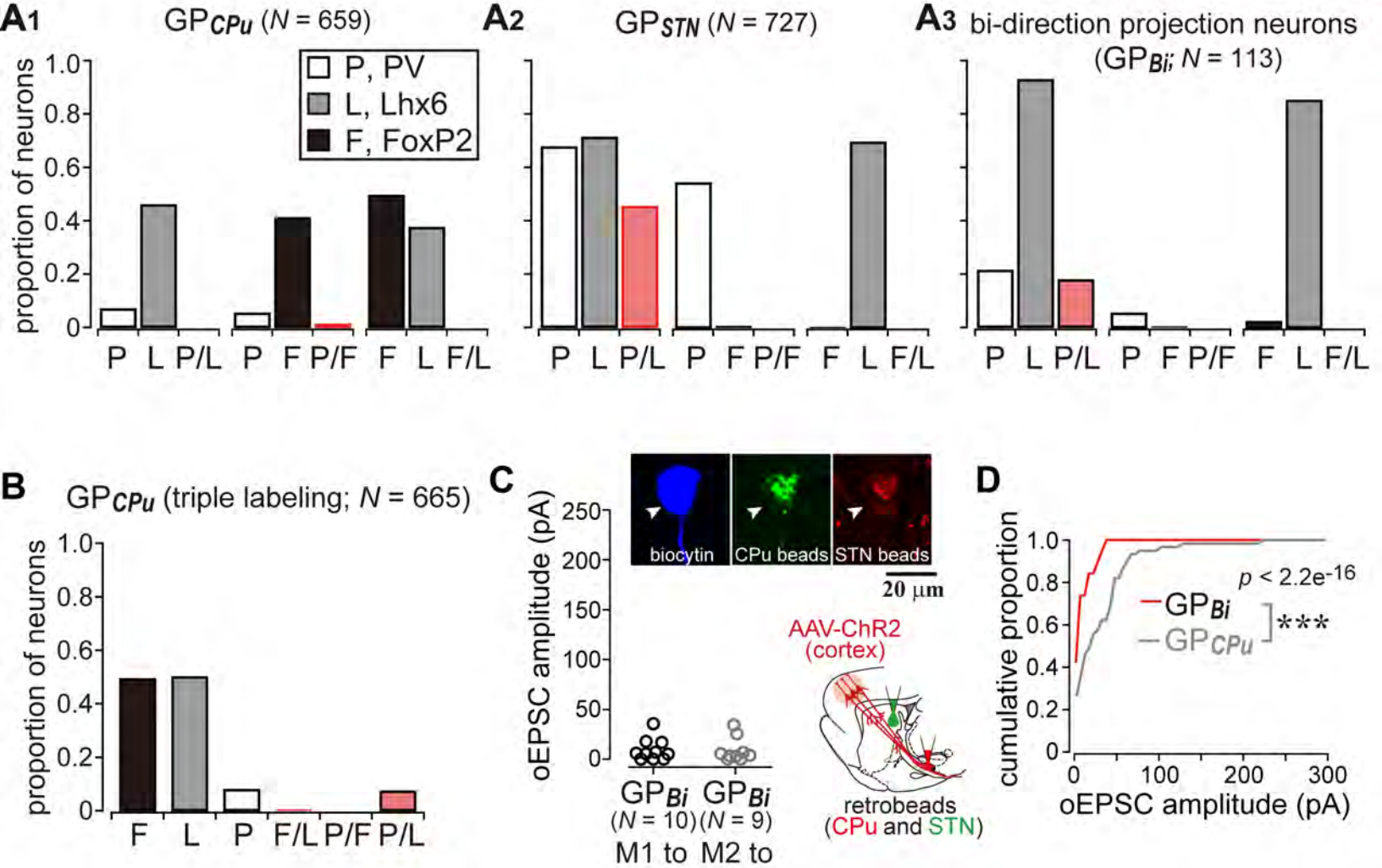

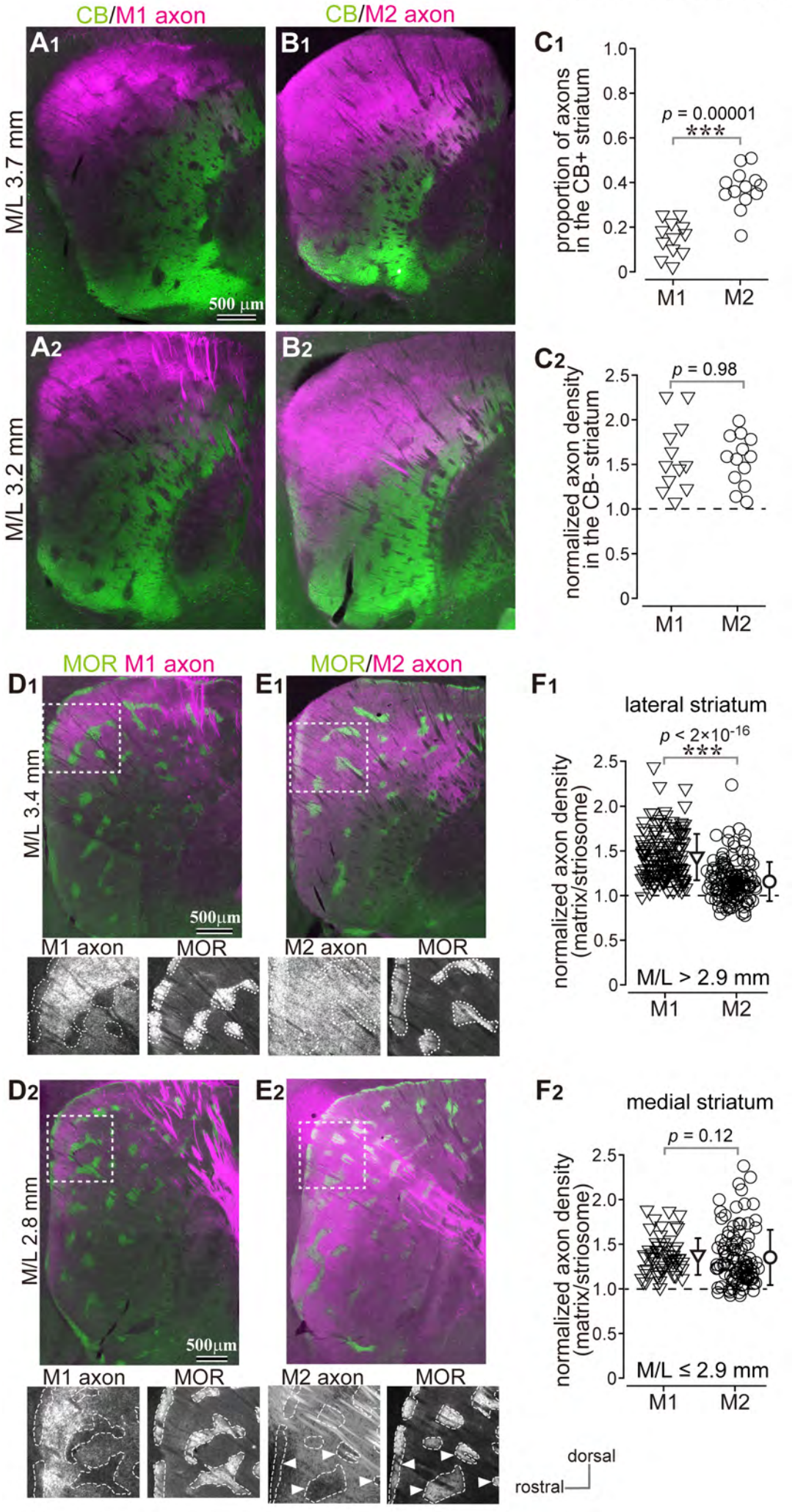
CB/M1 axon
CB/M2 axon
A1
B1
M/L 3.7 mm
500 μm
A2
B2
M/L 3.2 mm
C1
proportion of axons in the CB+ striatum
p = 0.00001
***
M1
M2
C2
normalized axon density in the CB- striatum
p = 0.98
MOR M1 axon
MOR/M2 axon
D1
E1
M/L 3.4 mm
500μm
M1 axon
MOR
M2 axon
MOR
F1
lateral striatum
p < 2×10-16
***
normalized axon density (matrix/striosome)
M/L > 2.9 mm
D2
E2
M/L 2.8 mm
F2
medial striatum
p = 0.12
M/L ≤ 2.9 mm
dorsal
rostral

Karube et al. 2019 Fig.7

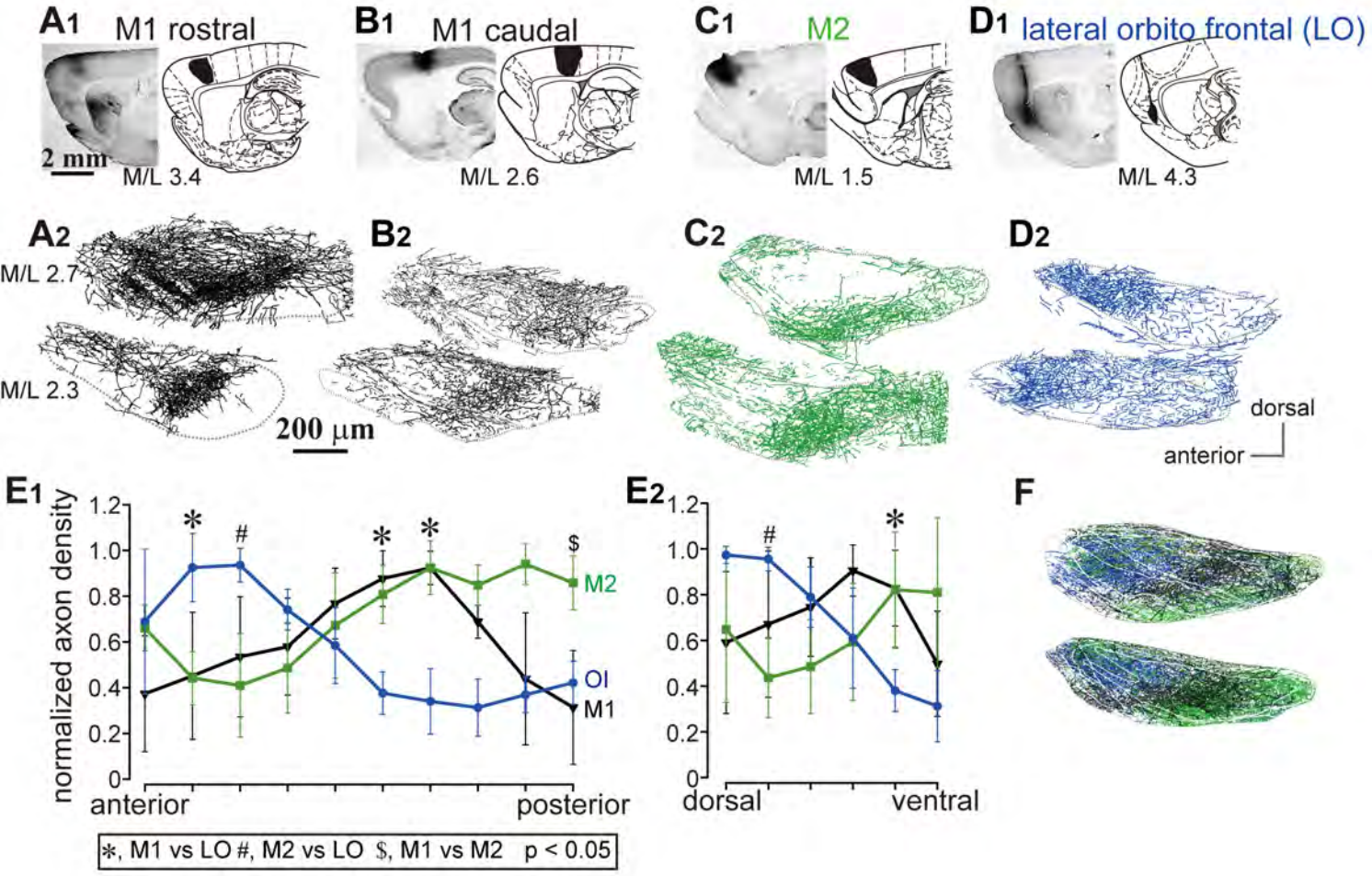

Karube et al. 2019 Fig. 8

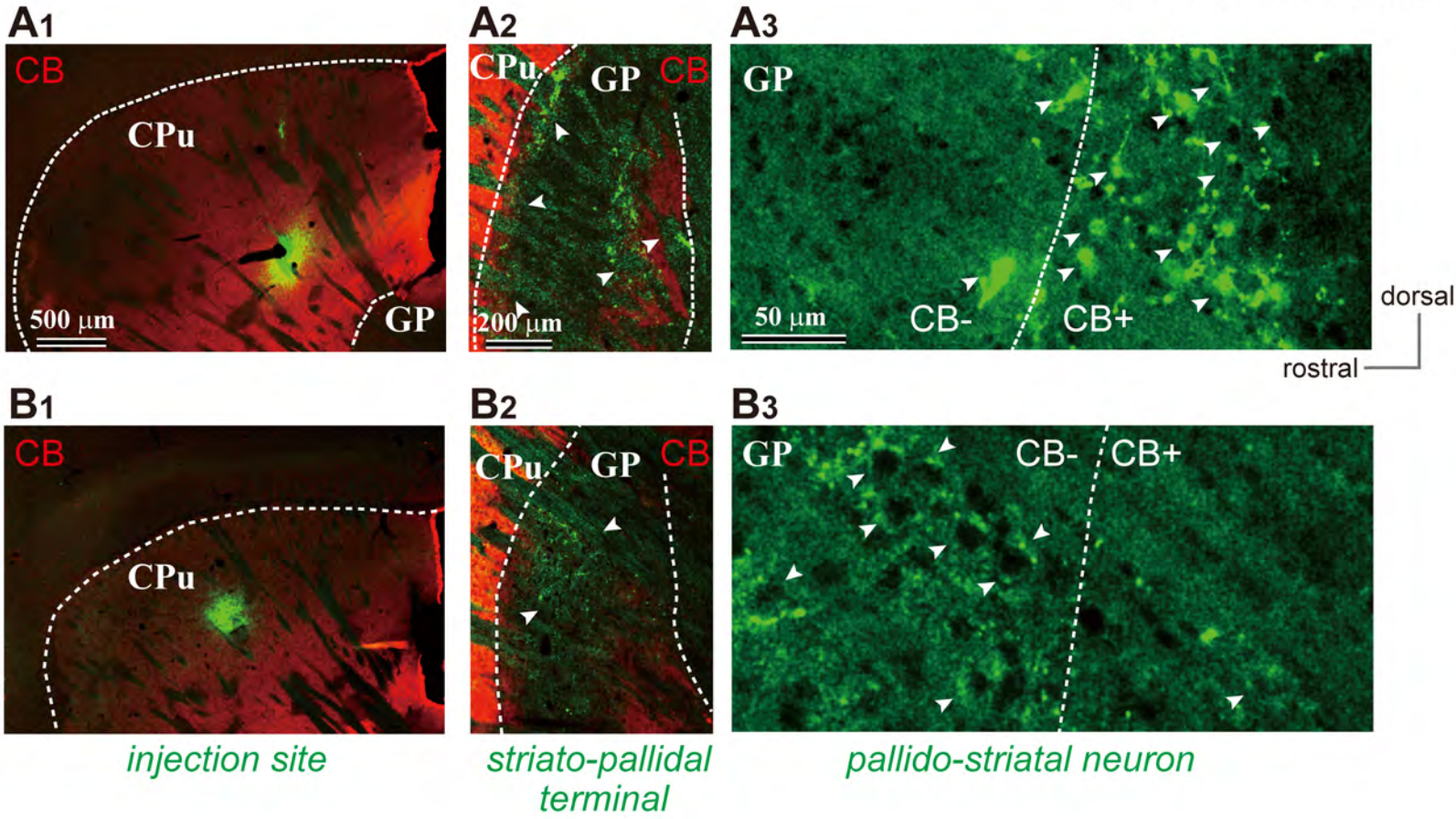

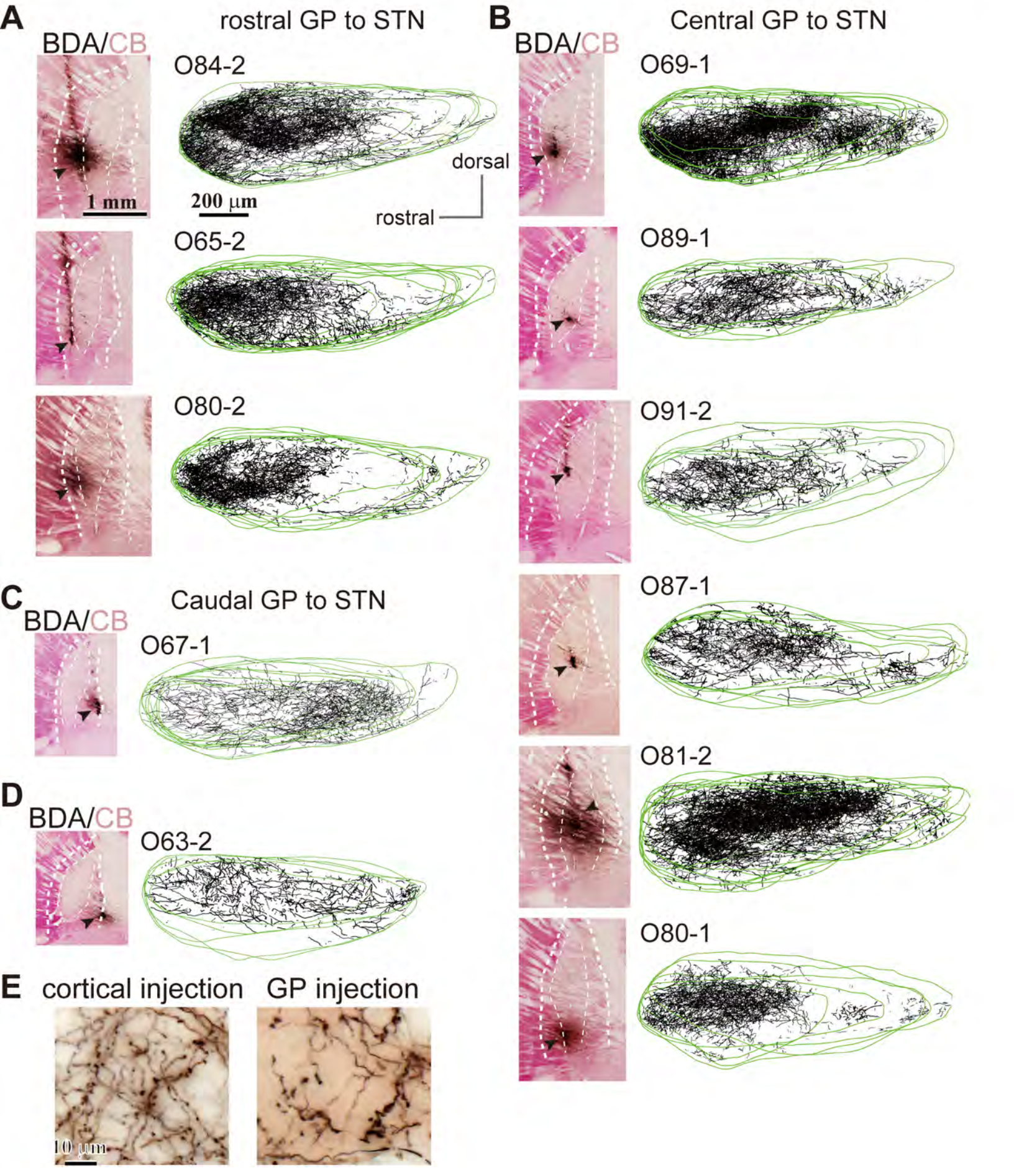
A
rostral GP to STN
BDA/CB
O84-2
1 mm
200 μm
dorsal
rostral
O65-2
O80-2
B
Central GP to STN
BDA/CB
O69-1
O89-1
O91-2
O87-1
O81-2
O80-1
C
Caudal GP to STN
BDA/CB
O67-1
D
BDA/CB
O63-2
E
cortical injection
GP injection
10 μm

Karube et al. 2019 Fig.10

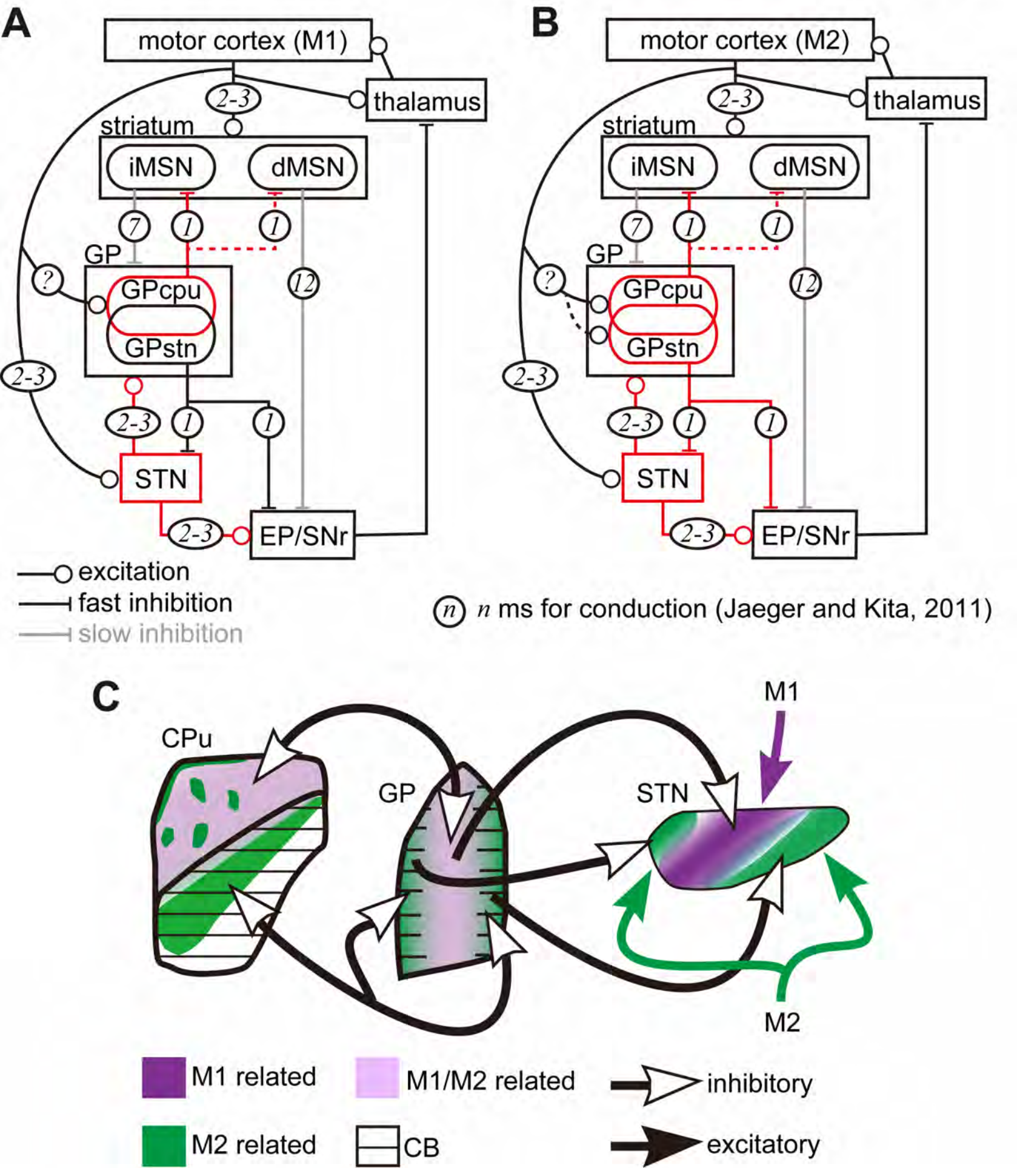

Karube et al. 2019 Fig.1-figure supplement 1

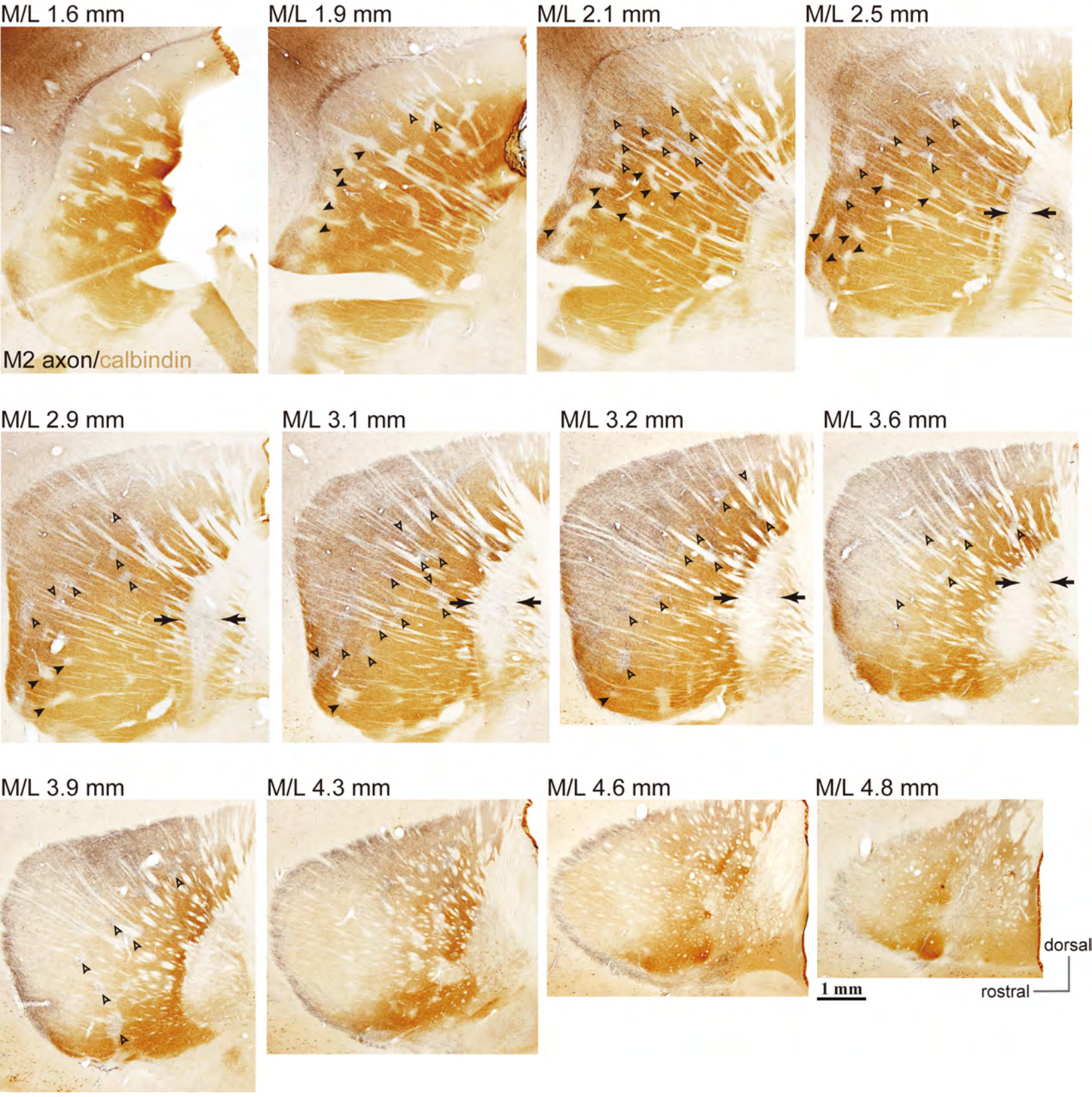

Karube et al. 2019 Fig.1-figure supplement 2

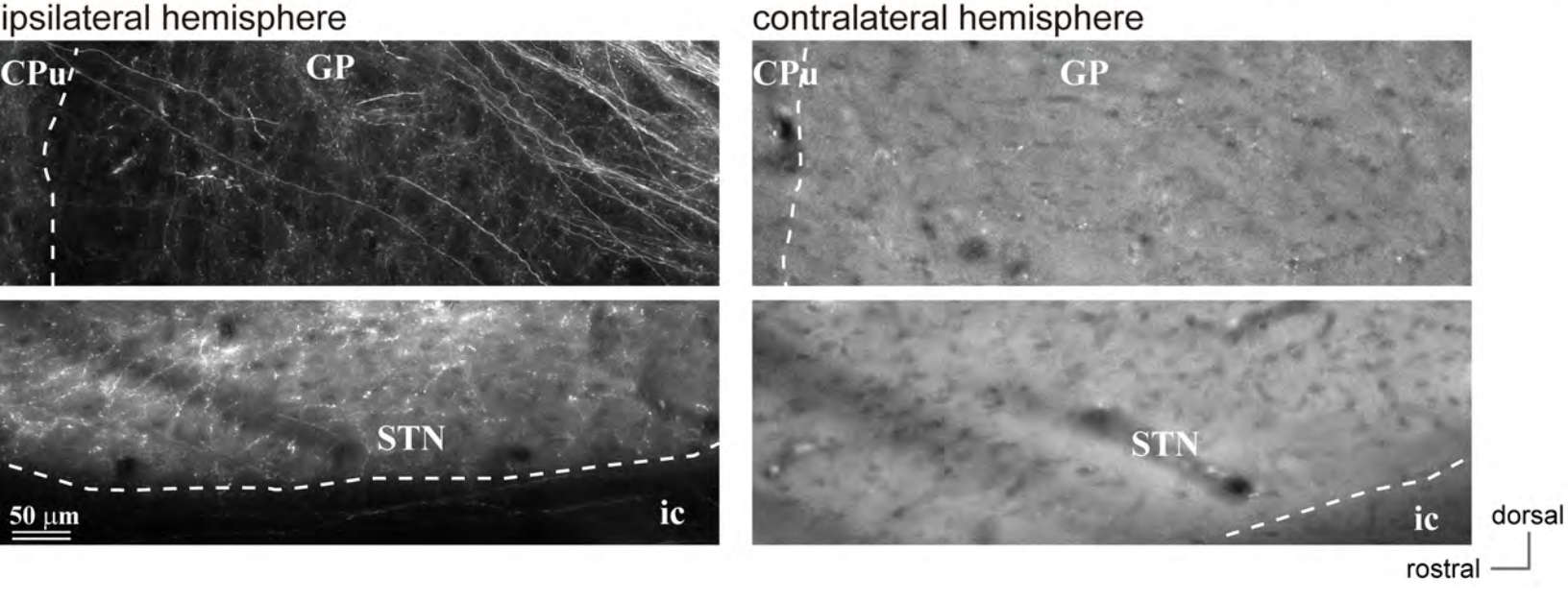

Karube et al. 2019 Fig.1-figure supplement 3

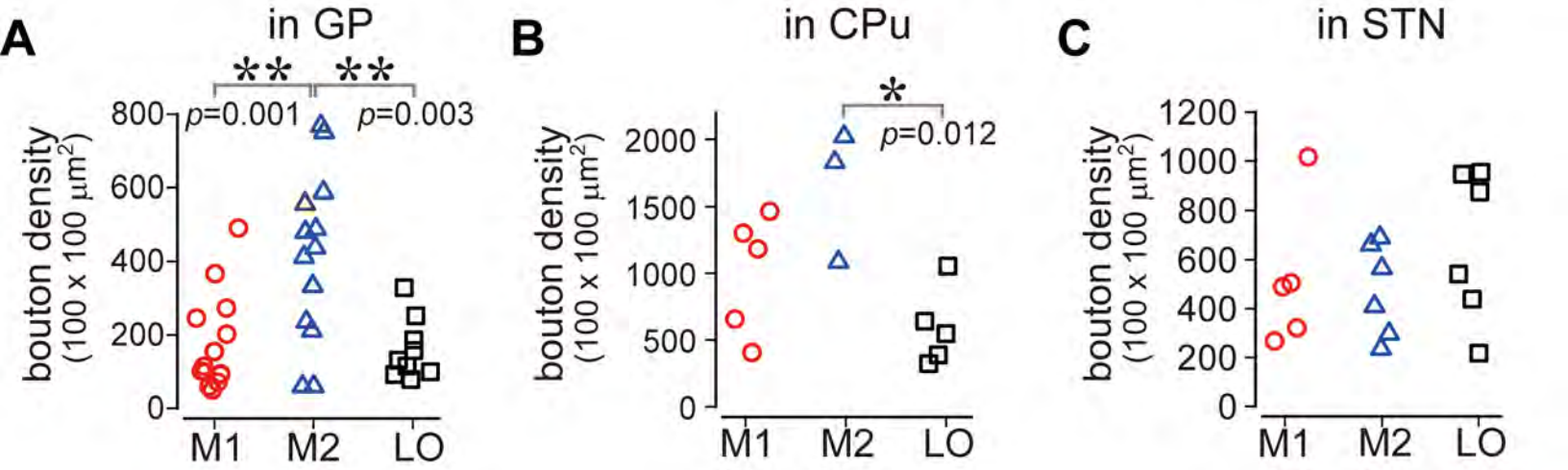

Karube et al. 2019 Fig. 7–figure supplement 1

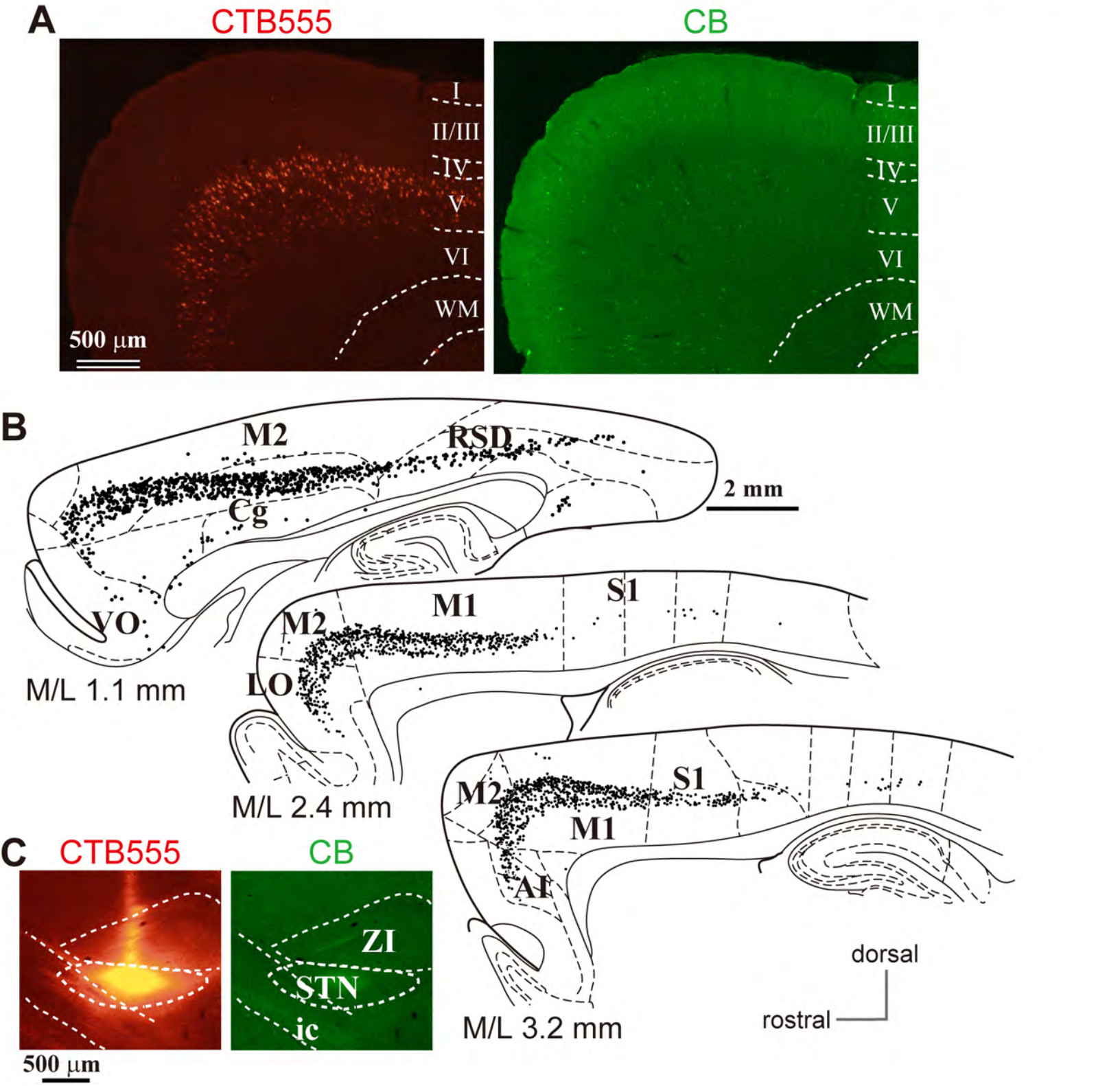

Supplementary materials

Orbitofrontal cortex (OFC) and anterior cingulate cortex (Cg) are involved in action (Schoenbaum et al., 2009). OFC provides behavioral flexibility via response inhibition and associative learning (but see previous reference). The OFC requires integration of sensory signals and internal states such as motivation with ongoing action selection and prediction of reward, to compute causal relationships between action selection and specific outcomes (Passingham & Wise, 2012). The Cg includes the rostral cingulate motor area (CMAr) (Morecraft & Van Hoesen, 1998), which lies in the cingulate sulcus, ventral to the presupplementary motor area, and in primates sends axonal projections to the spinal cord (Luppino, Matelli, Camarda, & Rizzolatti, 1994). The Cg and supplementary motor area (SMA) provide internal guides for action (Thaler, Chen, Nixon, Stern, & Passingham, 1995) correlated with motivation and voluntary behavior. The caudal cingulate motor area (CMAc), however, is preponderantly implicated in sensory-driven movement (Paus, 2001) and is thus related to action selection. Similarly to the OFC, the CMA promotes the switching of actions in response to changes in circumstances and internal desires (Amemori & Graybiel, 2012; Nakayama et al., 2015; Tanji, 1987), and is related to preparatory processes (Risterucci, Terramorsi, Nieoullon, & Amalric, 2003). CMAr projects to the M1, SMA, preSMA, premotor cortex, and brainstem,

including the pons and spinal cord (Sessle & Wiesendanger, 1982). The OFC and Cg have different cognitive functions in primates and rodents (Bissonette et al., 2008; Bissonette et al., 2013; Bissonette & Roesch, 2015; Friedman et al., 2015; Nakayama et al., 2015; Sul et al., 2010). Thus, the OFC and Cg are important for motor behavior as well as being motor areas, and we therefore investigated axon projections to the basal ganglia from lateral orbitofrontal cortex (LO) and rostral Cg.

Supplementary results

Cortico-striatal and cortico-pallidal projections from LO and anterior cingulate cortex (Cg)

For comparison, we investigated axons from LO and Cg, which are also located in the rat frontal cortex LO axons were distributed in the medio-ventral part of the striatum, whereas Cg axons were distributed in the medial striatum (Suppl Fig. 1, 2). LO axons were sparse in the dorsal striatum but dense in the caudal and ventral part of the dorsal striatum as well as in the nucleus accumbens. In addition, these axons preferentially innervated the striosomes (Suppl. Fig. 1, arrowheads). In contrast, Cg axons mainly projected to the dorsomedial striatum with preference for the CB(+) subregions, namely the matrix (Suppl. Fig. 2). To a degree, the spatial distribution of Cg axons was similar to

that of M2 axons; however, Cg axons did not preferentially project to the striosomes (Suppl. Fig. 2) (Averbeck, Lehman, Jacobson, & Haber, 2014; Friedman et al., 2015; Gabbott et al., 2005; Hintiryan et al., 2016).

LO axons also passed through the GP, but they branched less frequently, and axon collaterals were apparently not abundant (Suppl. Fig. 1). Actually, motor areas (both M1 and M2) provided more boutons than did LO, as expected based on the axon distribution. LO did not preferentially innervate the dorsal striatum or GP but preferred the nucleus accumbens, ventral pallidum, hypothalamus, and extended amygdala (Gabbott et al., 2005). LO projections to GP were not as dense as those to STN (Suppl. Fig. 1D1). The LO bouton density in the GP was approximately 30% of that in the striatum (Suppl. Fig. 1 D2). In contrast, the Cg projected to the medial GP and issued as many axon collaterals as did motor cortical areas (Suppl. Fig. 2).

Supplementary Figure legends

Supplementary Fig. 1. LO projections to the basal ganglia

(A) LO projections to the striatum. (A1) AAV injections into the LO. (A2) A representative LO projection to the striatum. LO axons (red) are distributed in the caudal and ventral part of the dorsal striatum (M/L 2.6 mm). (A3) Immunofluorescence for μ-

55 opioid receptor (MOR, green). Arrowheads indicate the striosomes, which are MOR(+),
56 innervated by the LO axons seen in A2 and A3. Dotted square areas in A2 and A3 are
57 magnified in the right-most column. (B) BDA injection into LO. (C) Brightfield images
58 of LO axons in GP, striatum (CPu), and STN. Note that axon and terminal densities in GP
59 were apparently lower than those in the striatum or STN. (E) Quantitative comparison of
60 axon density in the GP normalized with that in the STN (D1) and striatum (D2). See also
61 Fig. 1.
62
63 **Supplementary Fig. 2.** Cingulate cortex (Cg) projections to the basal ganglia
64 (A) Cg projections to the striatum (CPu) in sagittal sections (M/L 2.10 mm). Cg axons
65 are dense in the CB-negative subregions of the striatum. As in the case of M2 axons, Cg
66 axons were less dense in the CB-negative striosomes. (B) Cg projections to the GP. Cg
67 axon collaterals were dense in the CB(-) central GP. Thick axon bundles pass through the
68 dorsal side of the medial GP (M/L 2.4 mm). (C) Cg projections to the STN. Cg axons are
69 localized in the caudal part of the medial STN (arrowheads; M/L 2.4 mm).
70

71 **Suppl. Table 1.** Primary antibodies used in this study

Antigen	Host species	Supplier	Catalog number	RRID	Workin dilutio
Calbindin	mouse	Sigma	C9848	AB_476894	1:4000
Calbindin	rabbit	Frontier Institute	calbindin-Rb-Se-1	AB_2571568	1:2000
FoxP2	rabbit	Abcam	ab16046	AB_2107107	1:2000
Lhx 6	mouse	Santacruz	sc-271433	AB_10649856	1:1000
MOR	guinea pig	Millipore	AB1774	AB_91022	1:5000
MOR	rabbit	Neuromics	RA10104	AB_2156525	1:1000
PHA-L	goat	Vector	AS2224	AB_2315141	1:2000
Parvalbumin	mouse	Sigma	P3171	AB_2313693	1:4000
Parvalbumin	guinea pig	Synaptic Systems	195004/16	AB_2156476	1:5000

72 MOR, μ-opioid receptor; PHA-L, *Phaseolus vulgaris* leucoagglutinin

73

74 **Suppl. Table 2.** Secondary antibodies used in this study

Secondary antibody	Host species	Supplier	Catalog no.	RRID	Dilution
anti-rat Alexa Fluor®488	donkey	*	A21208	AB_141709	1:500
anti-mouse Alexa Fluor®546	donkey	*	A10036	AB_2534012	1:500
anti-mouse Alexa Fluor®635	goat	*	A31575	AB_2536185	1:500
anti-rabbit Alexa Fluor®405	goat	*	A31556	AB_221605	1:500
anti-rabbit Alexa Fluor®635	goat	*	A31577	AB_2536187	1:500
anti-guinea pig Alexa Fluor®405	goat	Abcam	ab175678	-	1:500
anti-guinea pig Alexa Fluor®594	goat	*	A11076	AB_141930	1:500

anti-guinea pig Alexa Fluor®633	goat	*	A21105	AB_2535757	1:500

All antibodies are polyclonal. * Thermo Fisher Scientific (Waltham, MA), Abcam (Cambridge, UK)

Supplementary References

Amemori, K., & Graybiel, A. M. (2012). Localized microstimulation of primate pregenual cingulate cortex induces negative decision-making. *Nat Neurosci, 15*(5), 776-785. doi:10.1038/nn.3088

Averbeck, B. B., Lehman, J., Jacobson, M., & Haber, S. N. (2014). Estimates of projection overlap and zones of convergence within frontal-striatal circuits. *J Neurosci, 34*(29), 9497-9505. doi:10.1523/JNEUROSCI.5806-12.2014

Bissonette, G. B., Martins, G. J., Franz, T. M., Harper, E. S., Schoenbaum, G., & Powell, E. M. (2008). Double dissociation of the effects of medial and orbital prefrontal cortical lesions on attentional and affective shifts in mice. *J Neurosci, 28*(44), 11124-11130. doi:10.1523/JNEUROSCI.2820-08.2008

Bissonette, G. B., & Roesch, M. R. (2015). Rule encoding in dorsal striatum impacts action selection. *Eur J Neurosci, 42*(8), 2555-2567. doi:10.1111/ejn.13042

Luppino, G., Matelli, M., Camarda, R., & Rizzolatti, G. (1994). Corticospinal projections from mesial frontal and cingulate areas in the monkey. *Neuroreport, 5*(18), 2545-2548.

Morecraft, R. J., & Van Hoesen, G. W. (1998). Convergence of limbic input to the cingulate motor cortex in the rhesus monkey. *Brain Res Bull, 45*(2), 209-232.

Risterucci, C., Terramorsi, D., Nieoullon, A., & Amalric, M. (2003). Excitotoxic lesions of the prelimbic-infralimbic areas of the rodent prefrontal cortex disrupt motor preparatory processes. *Eur J Neurosci, 17*(7), 1498-1508. doi:10.1046/j.1460-9568.2003.02541.x

Sessle, B. J., & Wiesendanger, M. (1982). Structural and functional definition of the motor cortex in the monkey (Macaca fascicularis). *J Physiol, 323*, 245-265.

Tanji, J. (1987). Neuronal acitivyin the primate non-primary cortex is different from that in the primary motor cortex. In R. Porter (Ed.), *Motor areas of the cerebral cortex.* (pp. 142-150). Chichester: Johm Wiley and Sons Ltd.

Thaler, D., Chen, Y. C., Nixon, P. D., Stern, C. E., & Passingham, R. E. (1995). The functions of the medial premotor cortex. I. Simple learned movements. *Exp Brain Res, 102*(3), 445-460.

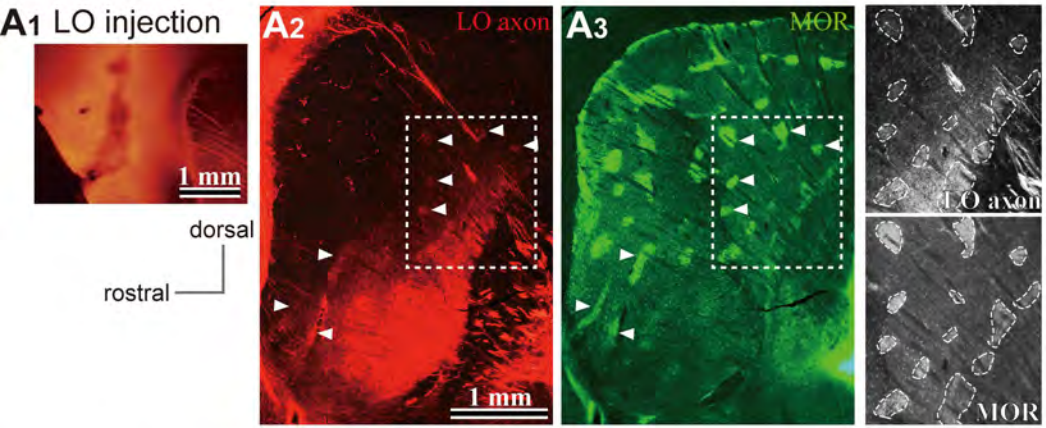
A1 LO injection
1 mm
dorsal
rostral
A2
LO axon
1 mm
A3
MOR
LO axon
MOR

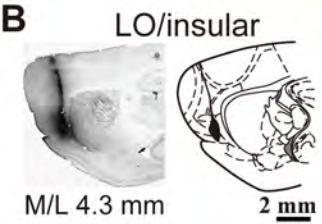
B
LO/insular
M/L 4.3 mm
2 mm

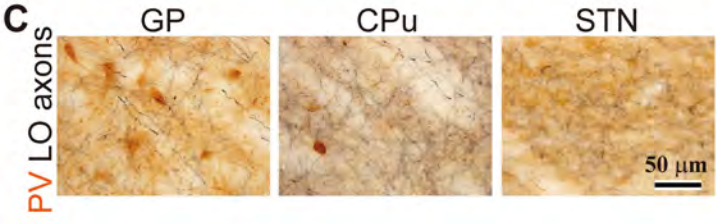
C
GP
CPu
STN
PV LO axons
50 μm

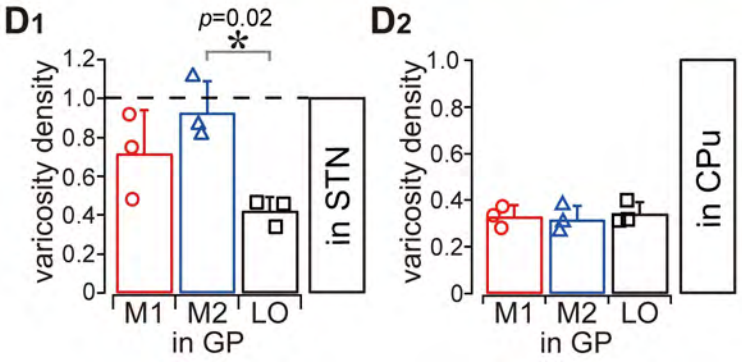
D1
p=0.02
*
varicosity density
1.2
1.0
0.8
0.6
0.4
0.2
0
M1
M2
LO
in GP
in STN
D2
varicosity density
1.0
0.8
0.6
0.4
0.2
0
M1
M2
LO
in GP
in CPu

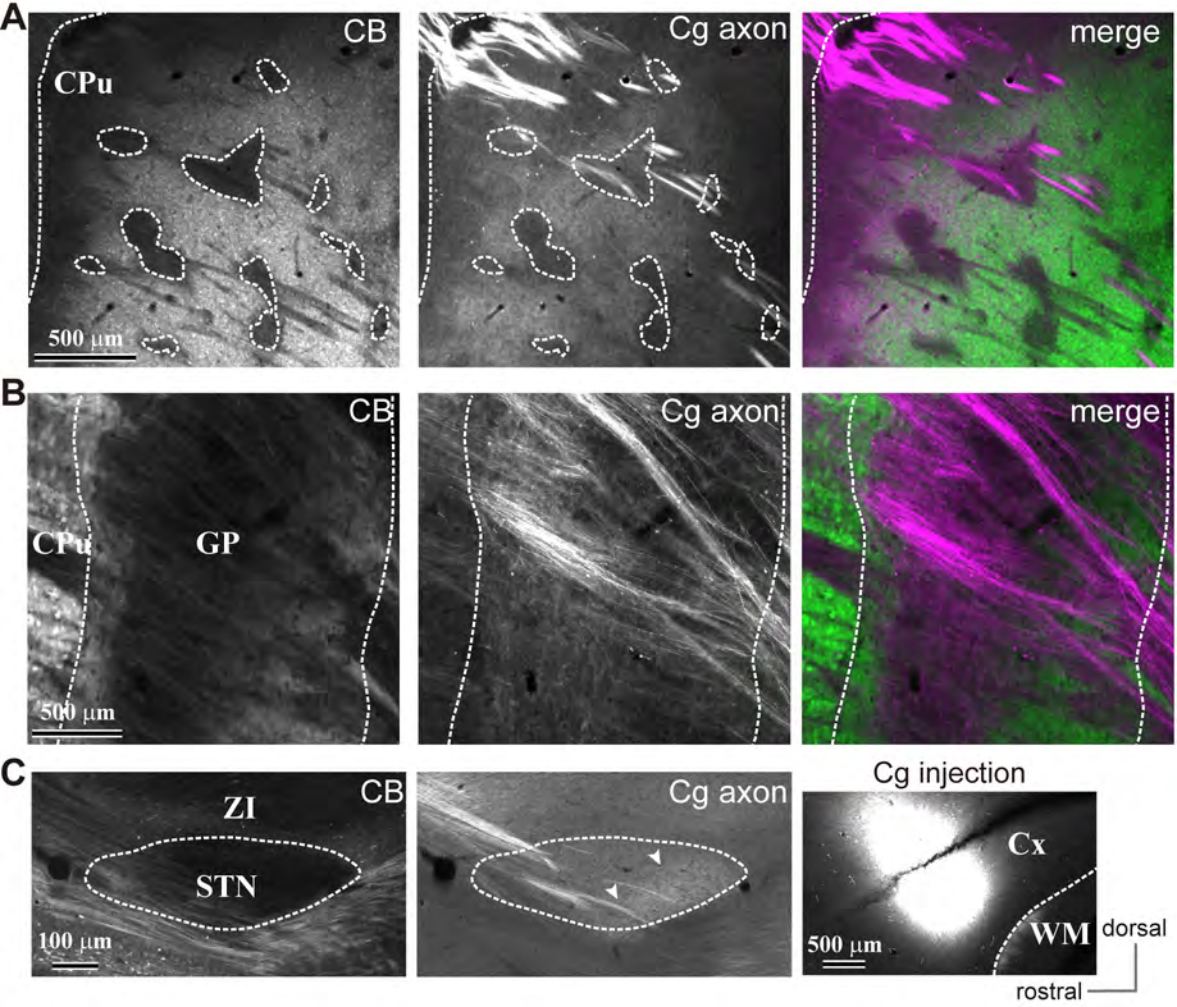
A
CB
CPu
500 μm
Cg axon
merge
B
CB
CPu
GP
500 μm
Cg axon
merge
C
CB
ZI
STN
100 μm
Cg axon
Cg injection
Cx
WM
500 μm
dorsal
rostral